MATERIALS STRUCTURE

in

Chemistry, Biology, Physics and Technology

STRUKTURA

2025

Kolokvium Krystalografické společnosti

Czech and Slovak
Crystallographic Association

vol. 31, no. 2, 2025

MATERIALS STRUCTURE

in Chemistry, Biology, Physics and Technology

Bulletin of the Czech and Slovak Crystallographic Association

www.xray.cz

STRUKTURA 2025

8.9.-12.9.2025

Hotel Concertino, Jindřichův Hradec

Struktura 2025 is organized again in South Bohemia but for the first time in Jindřichův Hradec. After two years it includes sessions on neutron scatering, that were prepared by recently established Czech Neutron Association. We can welcome guests from three European facilities. In addition, there are three short courses - again on the Mstruct software for fitting of some parameters of real structure; for biocrystallographers - Moorhen - web based application that brings the power of the COOT model-building software to the browser;and *mace-md-gui* that run basic molecular dynamic/static simulations in an interactive interface with a machine learning MACE MP interatomic potential. Nearly 70 registered participants are also invited to the excursion in museum of old American cars and brewery in Nová Bystřice, followed by raut in questhouse in Číměř that is owned by our former colleague -Anita Župčanová.

Electronic version of the journal can be found at http://www.xray.cz/ms together with the instructions for the authors.

R. Kužel

Supported by the Czech Academy of Sciences
Published by the Czech and Slovak Crystallographic Association (CSCA).
Technical editors: Ivana Kutá Smatanová, Radomír Kužel.
Supported by the Czech Academy of Sciences.
Printed by Karel Hájek, designhhstudio.
ISSN 1211 5894 (print), ISSN 1805-4382 (Online) volume **31** (September 2025), no. 2 @CSCA

DECTRIS

NEW

POLLUX

Versatile by Design
Exceptional by Performance

Designed for the lab, engineered for seamless integration, and built to deliver exceptional results – across every experiment.

Optimal energy resolution
for effective background suppression

Superior count rates
and unparalleled dynamic range

Large active area
up to 58 by 14 mm

Pixel detector
with 2D / 1D / 0D readout modes

Discover more
info@dectris.com

RIGAKU POWDER XRD SOLUTIONS

Wide range of solutions, from a cost-effective benchtop system to a multifunctional X-ray diffractometer (XRD)

SmartLab SE

MULTIPURPOSE X-RAY DIFFRACTION SYSTEM

- Most economical, multipurpose XRD system
- AutoAlign for all configurations and applications for always accurate data
- 6/10/48-position automated transmission and reflection sample changer
- Automatic optical component recognition ensures error-free handling

SmartLab

AUTOMATED MULTIPURPOSE X-RAY DIFFRACTOMETER

- Modular structure for all diffraction and scattering experiments with uncompromised performance in each application
- Automatic optical component recognition ensures error-free handling
- AutoAlign for all configurations and applications for always accurate data
- State-of-the-art X-ray detectors: D/teX Ultra 250 0D/1D, HyPix 400 and HyPix-3000 0D/1D/2D

MiniFlex XpC

COMPACT X-RAY DIFFRACTOMETER

- Compact high-power ultrafast theta-theta XRD system
- Robot or belt automation
- Best-in-class high-resolution data quality

MiniFlex

BENCHTOP POWDER X-RAY DIFFRACTION INSTRUMENT

- Most versatile benchtop XRD system
- Ambient and non-ambient experiments
- Multiple sample sizes and sample changer
- Powerful SmartLab Studio software

Rigaku
POWERING NEW PERSPECTIVES

Rigaku Europe SE | Hugenottenallee 167 | 63263 Neu-Isenburg | Germany | rigaku.com | info@rigaku.com

Loučná nad Desnou
18.-22.11. 2024

Struktura 2024

16. studentská přehlídka

STRUKTURA 2025

Jindřichův Hradec, 8.9.-12.9. 2025

Session I, September 8, Monday

L1

MINERALS WITHIN THE Pd-Ni-As SYSTEM: CRYSTAL STRUCTURES

F. Laufek[1], A. Vymazalová[1], D.A. Chareev[2], T.L. Grokhovskaya[3], V.V. Kozlov[3], J. Plášil[4]

[1]Czech Geological Survey, Geologická 6, Prague 5, Czech Republic
[2]Institute of Experimental Mineralogy, RAS, Chernogolovka, Moscow, Russia
[3]Institute of Geology of Ore Deposits, Petrology, Mineralogy and Geochemistry RAS, Moscow, Russia
[4]Institute of Physics ASCR, v.v.i., Na Slovance 2, 128 21 Prague 8, Czech Republic
frantisek.laufek@geology.cz

There are three ternary phases in the Pd-Ni-As system described as minerals, nipalarsite $Ni_8Pd_3As_4$, menshikovite $Pd_3Ni_2As_3$ and majakite, PdNiAs. Majakite and menshikovite were described as new minerals by Genkin [1] and Barkov [2], respectively. Their crystal structures have been hitherto unknown. Nipalarsite was described together with its crystal structure determination by Grokhovskaya et al. [3]. Majakite was found in intergrowths with other platinum minerals in chalcopyrite and thalnakhite ores of the Mayak mine (Talnakh deposit), menshikovite was discovered in mafic-ultramafic layered complexes Lukkulaisvaara and Chiney, Russia. A fragment of menshikovite extracted from a sample from Lukkulaisvaara intrusion, Russia, was used for a structure analysis of this mineral. As the natural majakite proved to be unsuitable for a structural analysis, crystal structure analysis was carried out on a synthetic analogue PdNiAs.

The synthetic analogues of minerals in the system and phases on a Pd_2As-Ni_2As join were prepared using the Kullerud´s evacuated silica-glass tube method. Pure elements were used as starting materials for synthesis. The evacuated tube with charges were heated at 400 °C for several weeks. In order to study the extent of the $(Pd,Ni)_{\Sigma 2}As$ solid solution, selected experiments at the Pd_2As-Ni_2As join were prepared at 450, 500, 520 and 540 °C. The experimental products were rapidly quenched in cold water and analysed by powder or single crystal X-ray diffraction and electron microprobe analysis.

The performed experiments revealed three structurally different phases (solid solutions) along the Pd_2As-Ni_2As join system at 450 °C: α-Pd_2As (*Cmc*2_1), β-$(Pd,Ni)_{\Sigma 2}As$ (*P*-62*m*) and $Pd_{1-x}Ni_{1+x}As$ (*Pnma*). The low-temperature orthorhombic phase α-Pd_2As transforms at 484 °C to a hexagonal phase and belongs to the to the high-temperature β-$(Pd,Ni)_{\Sigma 2}As$ solid solution.

The phase PdNiAs is at 450 °C part of the $Pd_{1-x}Ni_{1+x}As$ solid solution showing *Pnma* symmetry. Its crystal structure contains a mackinawite-like blocks of edge sharing $[NiAs_4]$ tetrahedra parallel to (001). Palladium shows unusual five-fold coordination resembling a tetragonal pyramid by As atoms. The coordination of Pd is further completed by close contacts with Ni and Pd atoms. Palladium atoms are located in voids between blocks of $[NiAs_4]$ tetrahedra. A phase transition from low-temperature orthorhombic phase to the high-temperature hexagonal phase was observed. The hexagonal phase PdNiAs was also described by Evstigneeva [4]. Menshikovite $Pd_3Ni_2As_3$ crystal structure contains deformed $[NiAs_4]$ tetrahedra. Each $[NiAs_4]$ tetrahedra shares one edge with one adjacent tetrahedra along the ***a***-axis and two opposing edges with adjacent tetrahedra along the ***c***-axis forming chains of edge-shared $[NiAs_4]$ tetrahedra running in 001 direction. Nickel atoms have three close contacts with adjacent Ni atoms across the shared tetrahedral edges. Palladium atoms show trigonal bipyramidal coordination by As atoms.

1. A. D. Genkin, T.L. Evstigneeva, N.V. Troneva, L.N. Valsov, *Int. Geol. Rev*., **20**, (1976), 96.
2. A. Y. Barkov, R.F. Martin, Y.A. Pakhomovsky, N.D. Tolstykh, A.P. Krivenko, *Can Mineral*., **40**, (2002), 679.
3. T. L. Grokhovskaya, O.V. Karimova, A. Vymazalová, F. Laufek, D.A. Chaarev, E.V. Kovalchuk, L.O. Magazina, V. A. Rassulov. *Min. Mag*., **83,** (2019), 837.
4. T. Evstigneeva, Y. Kabalov, J. Schneider. Material Science Forum, 321-324, (2000), 700.

This research was supported by the by the Strategic Research Plan of the Czech Geological Survey (DKRVO/ČGS 2023–2027).

L2

PHASE ANALYSIS OF SOIL SEDIMENTS WITH REGARD TO THE PRESENCE OF ASBESTOS MINERALS

Zdeněk Jansa, Štěpánka Jansová, Ján Minár

New Technologies Research Centre, University of West Bohemia in Pilsen, Pilsen

The aim of this work is to summarize current knowledge on the extensive issue of asbestos occurrence in general and in the Pilsen Region of the Czech Republic, to establish a suitable methodology for detecting the presence of naturally occurring asbestos in soil deposits in a given location based on experimental analyses motivated by analyses in other countries, and to accurately identify individual types of asbestos from a series of samples. Twelve samples were evaluated as part of this work, and this paper presents a summary of them. [1, 2]

The morphology and elemental composition of the studied samples were evaluated using scanning electron microscopy with an energy dispersive spectrum detector. Figure 1 shows examples of fibers resembling needles with very sharp ends, which morphologically corresponded to the amphibole group, and long, wavy fibers, which corresponded to the serpentine group.

The basic building block of the silicate structure of asbestos is the silicon-oxygen tetrahedron $[SiO_4]^{4-}$. Chrysotile, as a representative of the first group of asbestos - serpentines, is hydrated magnesium silicate and its stoichiometric chemical composition can be given as $Mg_3Si_2O_5(OH)_4$. However, it has been observed that the chemical composition of the fibrous phase is closely related to the composition of the surrounding rock matrix and can be highly variable, as can be seen in the overview of the summary formulas of asbestos compounds in Table 1. [3, 4, 5]

The chemical composition of minerals that make up the second group of asbestos—amphiboles—reflects the complexity of the environment in which they were formed and can vary considerably in terms of major and trace elements and other influences that contributed to their formation. Amphibole fibers can be considered a series of minerals in which one cation is gradually replaced by another. [6, 7]

The second method used was X-ray phase analysis. The samples were measured under identical conditions. The measurements were performed on a Panalytical X'Pert Pro powder diffractometer with a copper X-ray tube ($K_{\alpha 1}$ = 0.154 nm). An ultra-fast Pixcel semiconductor detector was used with evaluation in the High Score program. Standard symmetrical geometry with a Bragg-Brentano arrangement was used for the measurements.

The measurement range for all samples was set identically between 20 and 85° [2θ]. When evaluating the samples, it was found that the main diffraction lines are located within an angle of 40° [2θ], while other diffraction lines beyond this angle belong to the SiO_2 phase. Therefore, a section ranging from 20° to a maximum of 40° [2θ] was selected on all diffractograms.

Figure 2 shows the diffraction patterns of samples 1 and 2, before and after annealing, with the identified phases

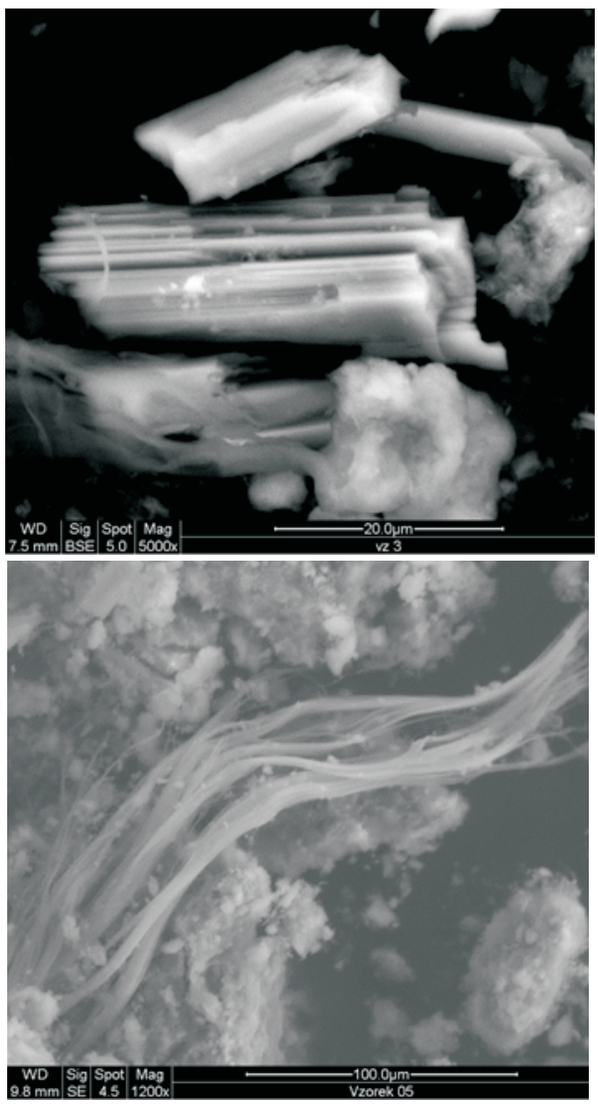

Figure 1. Images of samples 3 and 5.

marked in the range from 20 to a maximum of 40°[2θ]. The numerical designation of these phases corresponds to the numerical designation of the identified phases in Table 2.

Since the evaluation of the diffraction patterns of the unprocessed samples revealed a significant presence of organic components in the samples, all samples were annealed before further measurement. The samples were annealed at 530 °C for 4 hours and then cooled naturally. The temperature of 530 °C is below the thermal decomposition temperature of asbestiform minerals, so there was no loss of native information from the samples.

Scanning electron microscopy confirmed the presence of fibers that, from a morphological point of view, corre-

Table 1. Summarized formulas of asbestos compounds.

Chrysotile	$Mg_3Si_2O_5(OH)_4$
Amosite	$(Fe_2, Mg)_7Si_8O_{22}(OH)_2$
Crocidolite	$Na_2(Fe\ Mg)_3Fe_2Si_8O_{22}(OH)_2$
Antophylite	$(Mg, Fe_2)_7Si_8O_{22}(OH)_2$
Tremolite	$Ca_2Mg_5Si_8O_{22}(OH)_2$
Aktinolite	$Ca_2(Mg, Fe_2)_5Si_8O_{22}(OH)_2$

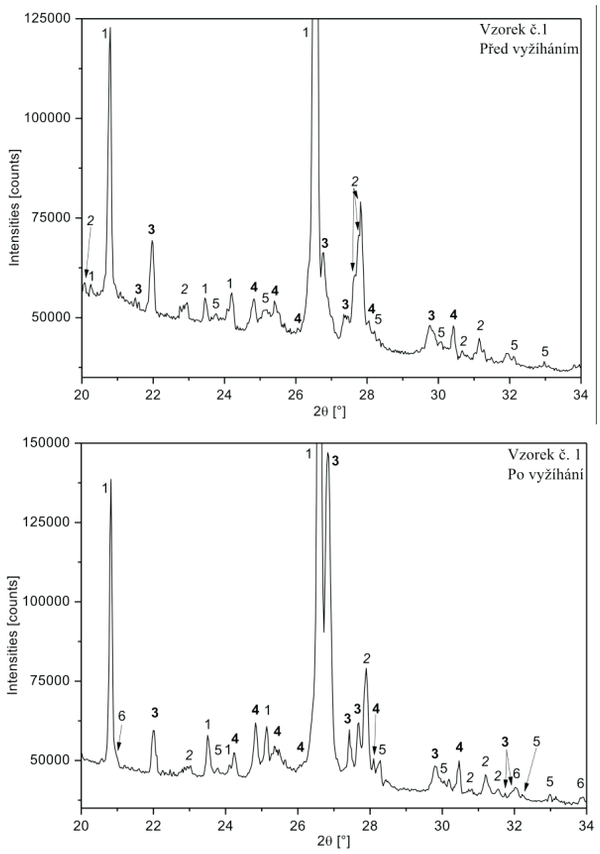

Figures 2. Evaluated diffractograms of sample 1 and 2 with identification of phases.

sponded to both main groups of asbestos minerals, namely the serpentine and amphibole groups. X-ray diffraction identified individual phases in the samples and determined the exact type of asbestos minerals found.

Table 2. Table of identified phases in soil sediment samples.

No	Mineral	Name of compound	Reference code	Chemical formula
1	quartz	silicon oxide	01-089-8935	SiO_2
2	---	magnesium silicate	01-086-0433	$Mg_2(Si_2O_6)$
3	antofylit	antofylite	96-901-6382	$Mg_{28}Si_{32}O_{96}$
4	chryzotil	chryzotile	96-101-0961	$Si_{16}Mg_{24}O_{72}$
5	wollastonit	calcium silicate	01-072-2297	$CaSiO_3$
6	---	hydrogen silicate	00-031-0581	$H_2Si_2O_5$

Table 3. Summary table of identified asbestos types

Sample ID	Chrysotile	Anthophyllite	Actinolite
S1:sample 1-2	x	x	x
S1:sample 3-4	x	x	x
S2:sample 1'-8'	x	x (except 6´)	x

After compiling the data from all analyses, we can say with certainty that chrysotile from the serpentine group is present in all evaluated samples. This is the least dangerous form of asbestos. Furthermore, we can say that the presence of anthophyllite from the amphibole group has been confirmed in all samples. Based on the morphology of the fibers, it is highly likely that crocidolite is also present in one sample, but this has not been confirmed by X-ray diffraction. The results of the asbestos found are shown in Table 3.

The combination of SEM analysis and X-ray diffraction provides a good set of tools for identifying asbestos. By gradually refining the measured diffraction pattern of the sample under investigation, it is possible to accurately determine the phases present, despite the complexity of the process.

1. F. Skácel, Z. Guschlová a V. Tekáč: Azbestová a minerální vlákna ve vnitřním ovzduší, Ústav plynárenství, koksochemie a ochrany ovzduší VŠCHT v Praze, Chemické listy 106, 961-970, 201.
2. Lajčíková, M. Hornychová: Azbest v ovzduší a legislativní zajištění ochrany zdraví, Státní zdravotní ústav Praha, 55(3), 99-101, 2010.
3. M. Novák: Mineralogický systém, prezentace [online – cit. 2021-12-06], Masarykova univerzita, available from: https://is.muni.cz/el/sci/podzim2011/G1061/Minera-I-system3a.pdf.
4. C. E. Housecroft, A. G. Sharpe: Anorganická chemie, ISBN 978-80-7080-872-6.
5. U.S. DEPARTMENT OF THE INTERIOR U.S. GEOLOGICAL SURVEY Asbestos: Geology, Mineralogy, Mining, and Uses by Robert L. Virta1, Open-File Report 02-149.
6. O.C. Wells: Scanning Electron Microscopy, McGraw-Hill, New York (1974).
7. M.Kužvart, Z. Weiss, Jílové materiály, jejich nanostruktura a využití, Praha červen 2005, ISBN 80-246-0868-5

L3

PROPERTIES OF SCHWERTMANNITE: THE CRITICAL ROLE OF PHASE PURITY

C. Pilloni[1], V. Mameli[2*], T. Kmječ[3], V. Gajdošova[4], C. Cannas[2], D. Zákutná[1*]

[1] *Department of Inorganic Chemistry, Charles University, Hlavova 2030, Prague 2 128 40, Czech Republic*
[2]*Department of Chemical and Geological Sciences, University of Cagliari, Cittadella Universitaria S.P. Monserrato Sestu Km 0.700, 09042 Monserrato, Italy*
[3]*Department of Low-Temperature Physics, Faculty of Mathematics and Physics, Charles University, V Holešovičkách 2, 180 00 Prague, Czech Republic*
[4]*Institute of Macromolecular Chemistry, Academy of Sciences of the Czech Republic, 162 06 Prague 6, Czech Republic*
valentina.mameli@unica.it, zakutnad@ill.fr

Schwertmannite, a poorly crystalline iron oxyhydroxysulphate, is an iron-bearing mineral that plays a pivotal role in various environmental processes, particularly in the treatment of acidic mine drainage [1]. Due to its ability to adsorb metal ions, anions, and its high surface area-to-volume ratio, schwertmannite has drawn significant attention as a potential medium for mitigating environmental contamination [2]. However, its poorly crystalline structure presents significant challenges in characterising its composition, making it difficult to detect and to quantify trace impurities. One such impurity is goethite, another iron mineral that can form under similar conditions due to higher thermodynamic stability [3]. Differentiating between schwertmannite and goethite in environmental or

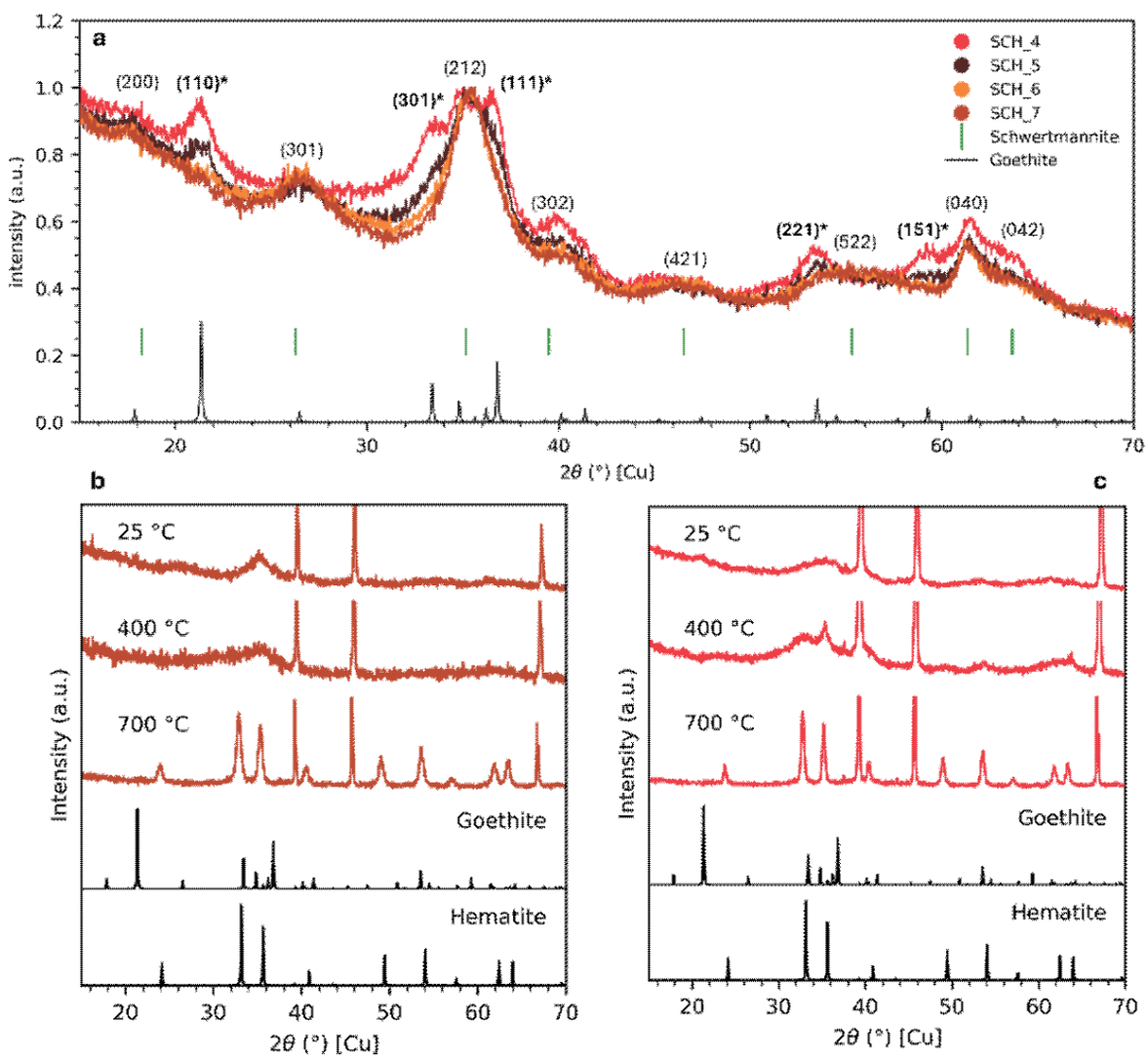

Figure 1. a) room temperature powder x-ray diffraction pattern of all the samples, high-temperature powder x-ray diffraction pattern of: b) SCH4, sample richer in goethite, and c) SCH7, purest sample.

synthetic samples is crucial, as the presence of goethite affects the chemical reactivity and stability of schwertmannite, thereby altering its efficiency in ecological applications. The aim of this study is to characterise four synthetic samples of schwertmannite with different levels of goethite impurity. The presence was detected using a combination of Room-Temperature Powder X-ray Diffraction (RT-PXRD) and High-Temperature Powder X-ray Diffraction (HT-PXRD), Fourier Transform Infrared spectroscopy in Attenuated Total Reflectance mode (ATR-FTIR), and Thermogravimetric Analysis (TGA), with characteristic features in all the techniques. Notably, increasing precursor concentration led to decreased goethite content in the samples, as evidenced by the progressive disappearance of diffraction maxima observed from RT-PXRD (**Fig. 1a**). This is further confirmed by the presence of the hematite diffraction maxima after 400 °C in the samples richer in goethite (**Fig. 1b, c**). Interestingly, only magnetisation measurements provide information on the presence of goethite in the purest sample, demonstrating it as a powerful probe for this poorly crystalline system. These findings confirm that magnetic characterization based on Vibrating Sample Magnetometer (VSM) can serve as an effective tool for identifying goethite impurities in schwertmannite, thereby contributing to the knowledge of poorly crystalline iron materials, and highlighting the potential of magnetic techniques for enhancing our comprehension of these materials in both natural and engineered systems.

1. J. M. Bigham, U. Schwertmann, S. J. Traina, R. L. Winland, and M. Wolf, ‘Schwertmannite and the chemical modeling of iron in acid sulfate waters’, *Geochim. Cosmochim. Acta*, vol. 60, no. 12, pp. 2111–2121, Jun. 1996, doi: 10.1016/0016-7037(96)00091-9.

2. B. Marouane *et al.*, ‘The potential of granulated schwertmannite adsorbents to remove oxyanions (SeO32-, SeO42-, MoO42-, PO43-, Sb(OH)6-) from contaminated water’, *J. Geochem. Explor.*, vol. 223, p. 106708, Apr. 2021, doi: 10.1016/j.gexplo.2020.106708.

3. P. Acero, C. Ayora, C. Torrentó, and J.-M. Nieto, ‘The behavior of trace elements during schwertmannite precipitation and subsequent transformation into goethite and jarosite’, *Geochim. Cosmochim. Acta*, vol. 70, no. 16, pp. 4130–4139, Aug. 2006, doi: 10.1016/j.gca.2006.06.1367.

L4

IMPROVING THERMOELECTRIC EFFICIENCY OF MULTILAYER ScN/$Sc_{1-x}Nb_xN$ HETEROSTRUCTURES BY Nb DOPING

Joris More-Chevalier[1], Urszula. D. Wdowik[2], Jiří Martan[3], Xavier Portier[4], Stanislav Cichoň[1], Esther de Prado[1], Petr Levinský[1], Ladislav Fekete[1], Jan Pokorný[1], Dejan Prokop[1,5], Petr Hruška[1,5], Markéta Jarošová[1], Jan Kejzlar[1], Dominik Legut[2,5], Michal Novotný[1], Ján Lančok[1]

[1]Institute of Physics of the Czech Academy of Sciences, Na Slovance 2, 18221 Praha 8, Czech Republic

[2]IT4Innovations, VSB - Technical University of Ostrava, 17. listopadu 2172/15, CZ 708 00 Ostrava-Poruba, Czech Republic

[3]New Technologies Research Centre (NTC), University of West Bohemia, Univerzitni 8, 301 00 Plzeň, Czech Republic

[4]CIMAP Normandie Université, ENSICAEN, UNICAEN, CEA, UMR CNRS 6252, 6 Boulevard Maréchal Juin, 14050 Caen Cedex 4, France

[5]Faculty of Mathematics and Physics, Charles University, Ke Karlovu 3, 121 16 Prague 2, Czech Republic

The thermoelectric properties of ScN/$Sc_{1-x}Nb_xN$ multilayers deposited on MgO (001) substrates were investigated using a combined experimental and theoretical approach based on the density functional theory. Four multilayers were prepared, exhibiting total Nb percentages of 0.4 %, 1.2 %, 1.8 %, and 4.8 % atomic ratio in the samples. Structural characterization confirmed the epitaxial growth of multilayers with sharp interfaces. Thermoelectric measurements showed an enhancement of the Seebeck coefficient and a reduction in thermal conductivity with Nb-doped ScN interlayers. The figure of merit *(ZT)* was potentially increased to over 0.3. This improvement highlights the promise of this approach for enhancing the thermoelectric performance of scandium nitride.

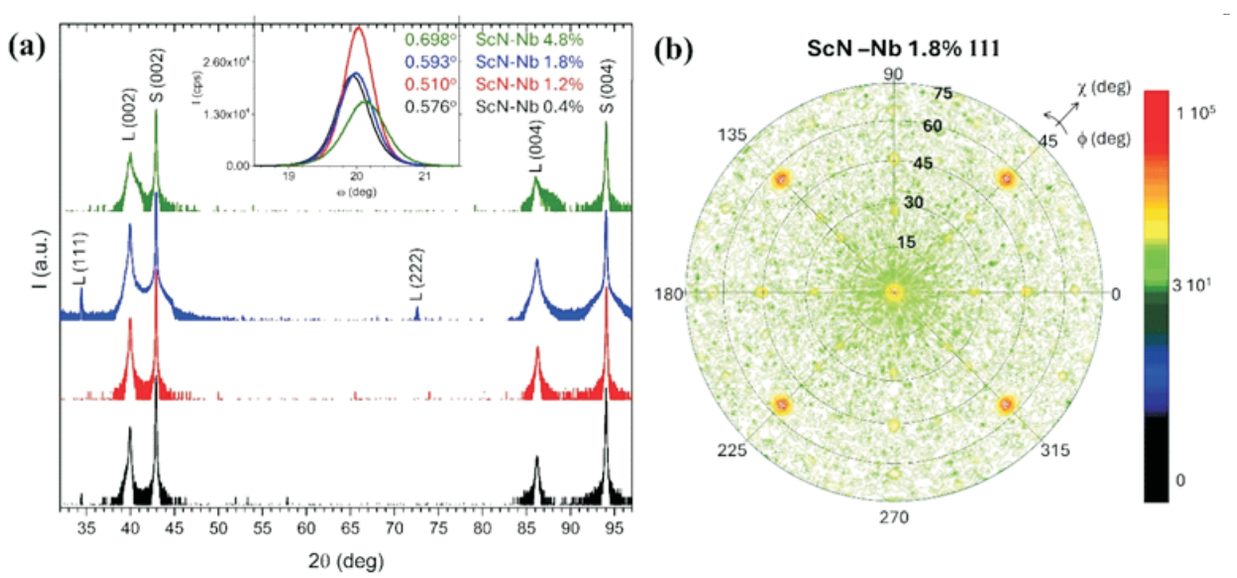

Figure 1. In (a), the 2θ/ω scans of each ScN-Nb film in the 2θ range from 30° to 100°. The inserts include the 002 rocking curves of each film, including the FWHM, which are equal to 0.576°, 0.510°, 0.593°, and 0.698° for the multilayer films containing 0.4%, 1.2%, 1.8%, and 4.8% of Nb, respectively. In (b), 111 pole figure of the ScN-Nb 1.8%.

L5

TENKÉ VRSTVY $BaTiO_3/LaNiO_3$: OD DIFRAKCE K POČÍTAČOVÝM SIMULACÍM

J. Drahokoupil[1,2,3], M. Lebeda[1,2,3], J. Remsa[1]

[1]Fyzikální ústav, Akademie věd České Republiky, Na Slovance 2, 182 21 Praha 8, Česká Republika
[2]Katedra inženýrství pevných látek, Fakulta jaderná a fyzikálně inženýrská v Praze, České vysoké učení technické v Praze, Technická 4, 166 07 Praha 6 - Dejvice, Česká Republika
[3]Ústav fyziky, Fakulta strojní, České vysoké učení technické v Praze, Technická 4, 166 07 Praha 6 - Dejvice, Česká Republika
draho@fzu.cz

Barium titanát, $BaTiO_3$ (BTO) je klíčový materiál v moderní elektronice, kde má velmi široké uplatnění díky svým feroelektrickým, dielektrickým a piezoelektrickým vlastnostem. Další zajímavou látkou je $LaNiO_3$ (LNO), který je jako jeden z mála perovskitů vodivý i při pokojové teplotě, a proto nachází uplatnění např. v tenkých vrstvách v kombinaci s ostaními perovskitovými materiály. Tento příspěvek se bude věnovat charakterizaci a teoretickým předpovědím směsného perovskitu BTO/LNO, který byl připraven ve formě tenkých vrstev na křemíkovém substrátu. Pro přípravu těchto vrstev byl použit unikátní systém skládající se s klasického PLD (pulzní laserová depozice) systému obohaceného o druhý terč v tzv. "off-axis" poloze. Snaha o přípravu objemových vzorků vede většinou ke vzniku více fází. Ač se na první pohled tyto dva krystalické systémy liší, viz obr. 1 – BTO bývá při pokojové teplotě v pseuduokubické struktuře s malou tetragonální výchylkou a LNO má při pokojové teplotě rhobohedrickou strukturu jsou difrakční záznamy těchto dvou perovskitů podobné. Při vhodné volbě mřížových parametrů dokonce těžko rozlišitelné – viz obr. 2.

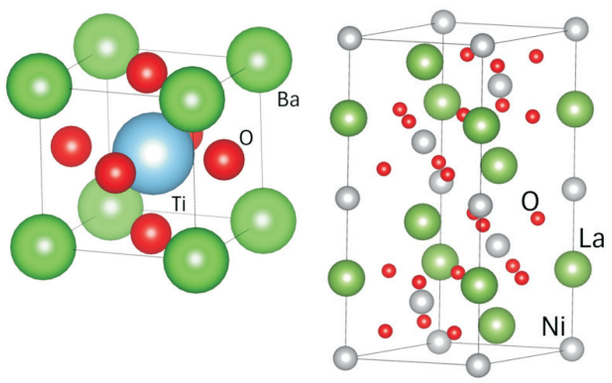

Obrázek 1. Krystalová struktura $BaTiO_3$ (vlevo) a $LaNiO_3$ (vpravo).

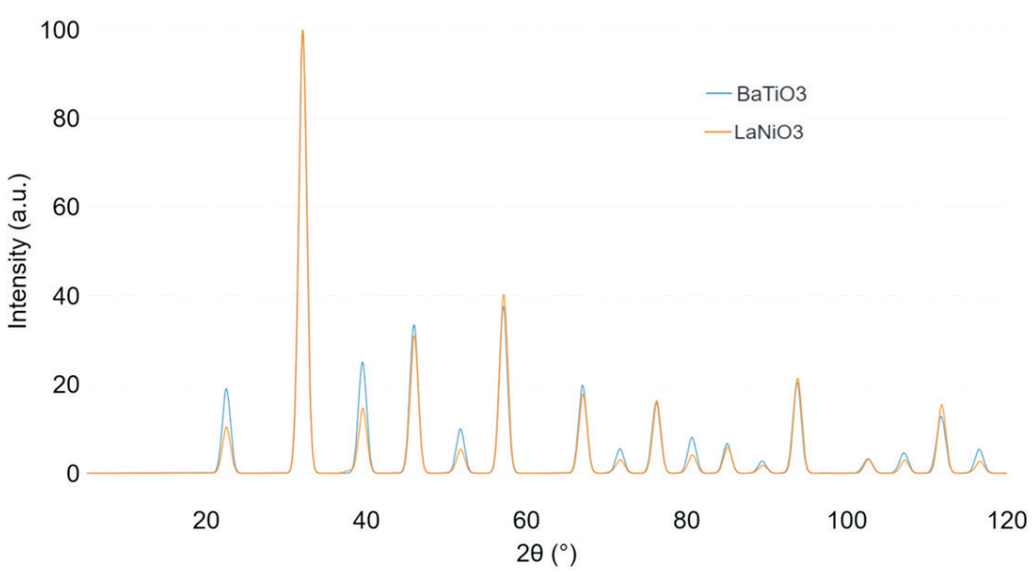

Obrázek 2. Teoretické difrakční záznamy pro $BaTiO_3$ (P4*mm* - *a* = 3,943, *b* = 3,958) a $LaNiO_3$ (R-3cH - a = 5,578, c = 13,677). (Nagenerováno pomocí programu XRDlicious)

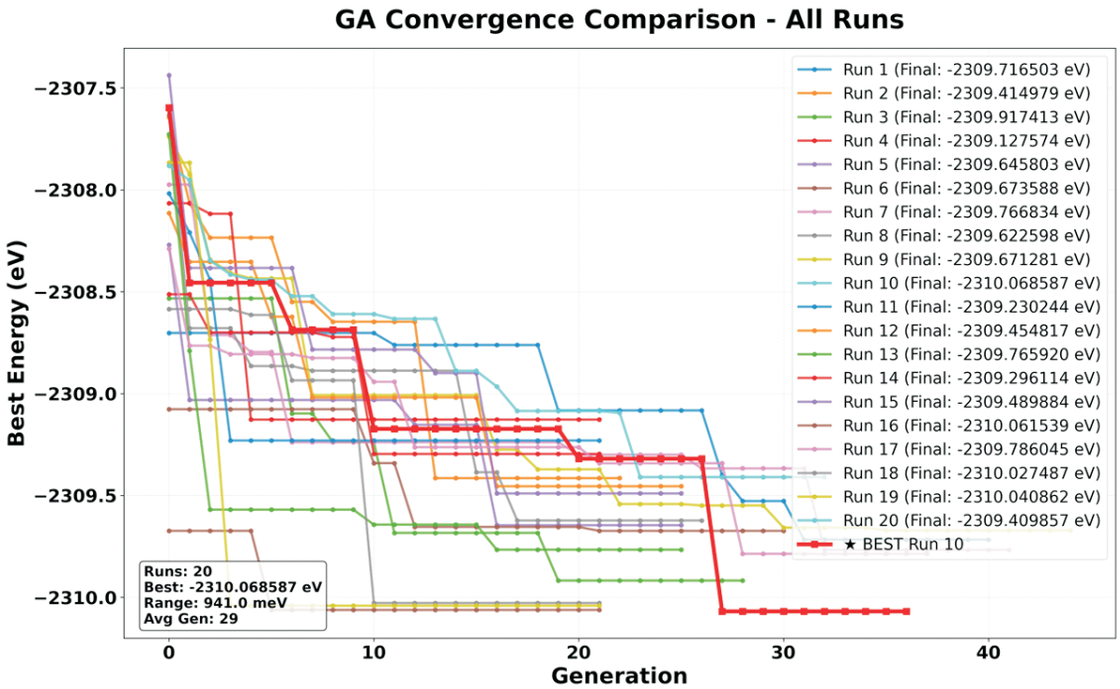

Obrázek 3. Několik běhů genetického algoritmu s cílem najít energeticky nejvýhodnější obsazení atomových pozic – výstup z programu MACE GUI.

Připravené vrstvy s různou koncentrací BTO či LNO vykazují krystalickou formu a difrakční záznam ukazuje, v rámci svého rozlišení, na jednu krystalickou mřížku. Vzhledem k pozorovanému rozšíření dikrakčních píků rozlišit nelze velmi podobné mřížky rozlišit a nelze vyloučit separaci na části bohatší na Ba resp. La.

Kromě různých experimentální technik byl tento systém studováni také pomocí DFT výpočtů a pomocí strojově naučeného (na DFT data) meziatomové potenciálu MACE a jeho implementaci do námi vytvořeného (nejenom) grafického rozhraní MACE GUI. Kromě výpočtu mřížkových parametrů jsme se zajímali i o energetickou výhodnost obsazovaní konkrétních atomových pozice různými prvky.

Na obr. 3 je zobrazeno několik běhů genetického algoritmu s cílem najít vhodné rozmístění Ba/La a Ti/Ni v superbuňce obsahující 320 atomů. Superbuňka vycházela z tetragonální struktury BTO a předpokládali jsme, že La obsazuje stejnou atomovou pozici jako Ba a Ni stejnou atomovou pozici jako Ti. Mřížkové parametry pro studovanou koncentraci 50:50 byli převzaté z experimentální dat a geometrická optimalizace pozic atomů či velikosti superbuňky nebyla prováděna. Je patrné, že pro takto velkou superbuňku nebylo velmi pravděpodobně nalezeno globální minimum, protože každý běh dopadl jinak.

Session II, September 8, Monday

L6

LIGHT INDUCED HALIDE SEGREGATION IN MIXED-HALIDE PEROVSKITES

P. Machovec[1], L. Horák[1], M. Dopita[1], V. Holý[1,2]

[1]Faculty of Mathematics and Physics, Charles University, Ke Karlovu 5, 121 16 Prague 2, Czech Republic,
[2]Institute of Condensed Matter Physics, Masaryk University, Kotlářská 2, 611 37 Brno, Czech Republic,
petr.machovec@matfyz.cuni.cz

Mixed-halide perovskites (MHPs) exhibit tunable band gaps, making them attractive for tandem photovoltaic applications. However, under illumination, halide ions migrate and segregate into iodine- and bromine-rich regions, reducing device efficiency. Here, we present a quantitative X-ray diffraction (XRD) approach for resolving the spatial distribution of halide ions during and after illumination. We present a model linking local composition fluctuations to strain fields, atom displacements, and diffuse scattering, enabling fitting of measured diffraction profiles from polycrystalline $FA_{0.83}Cs_{0.17}Pb(I_{0.6}Br_{0.4})_3$ thin films and $FA_{0.83}Cs_{0.17}Pb(I_{0.85}Br_{0.15})_3$ single crystals.

Illumination experiments were conducted using a solar simulator at 1 Sun equivalent, with diffraction patterns measured before and after 10 min and 30 min light exposures, followed by relaxation in darkness for up to two days. The concentration of Br within the sample was modelled by a random function with a correlation function $\sigma^2 \exp\left(-\frac{|\vec{r}-\vec{r}'|}{\xi^2}\right)$ and the experimental data were fitted using model of X-ray scattering, with parameters including the root mean square (rms) Br concentration deviation σ, correlation length ξ grain radius R, and asymmetry factor α.

In pristine polycrystalline samples, diffraction peaks were symmetric, consistent with a cubic perovskite lattice with mean grain radius of 50 nm. Illumination induced asymmetric broadening toward higher diffraction angles, increasing with scattering angle, and accompanied by slight peak shifts to lower 2θ. The fits revealed a significant rise in σ during illumination, indicating enhanced fluctuations in local composition, followed by slow partial relaxation in darkness within tens of hours. The asymmetry factor á remained consistently > 5, which is the limit of sensitivity of our model to this parameter, indicating the formation of highly bromide-rich regions embedded in a slightly iodine-rich matrix—an observation not previously observed by optical probes such as photoluminescence, which reported I-rich domains. The correlation length was found to be ≥ 15 nm and unaffected by illumination cycles.

For the single crystal samples reciprocal space maps were measured before and after 30 minutes of light soaking. We attempted fitting the data with the same correlation function as the polycrystalline samples, but the shape of the diffraction maxima can't be properly fitted. A distribution of the Br concentration consisting of Br-rich spheres in slightly I-rich volume was used to achieve good fit.

The results suggest that illumination drives preferential outward migration of I^- ions from nucleation sites such as grain boundaries or defects, leading to the observed microstructure. The method provides quantitative, bulk-sensitive insight into light-induced halide segregation, complementing surface-sensitive optical techniques. It also highlights the incomplete reversibility of segregation. This quantitative diffraction-based approach offers a new pathway to investigate ionic migration and microstructural evolution in perovskite optoelectronic materials.

L7

THIOPHENE-BASED CONDUCTIVE POLYMERS: STRUCTURAL ORDER VS. CONDUCTIVITY

Dominik Farka

Faculty of Science, University of South Bohemia in České Budějovice, Czech Republic
farka@prf.jcu.cz

Polythiophenes dominate the field of conductive polymers. This is in particularly true for the renowned PEDOT, where particularly outstanding charge-transport properties were observed. In this talk, three, state-of-the-art conductive polymers synthesized via tube-furnace oxidative chemical vapour deposition (oCVD) are presented. We will focus on the role of substitution-effects, the role of the counter-ion in achieving large crystallites in thin-films and related charge transport. Alternative emerging methods will be discussed in terms of an outlook.

1. Farka, D.; Coskun, H.; Gasiorowski, J.; Cobet, C.; Hingerl, K.; Uiberlacker, L. M.; Hild, S.; Greunz, T.; Stifter, D.; Sariciftci, N. S.; Menon, R.; Schoefberger, W.; Mardare, C. C.; Hassel, A. W.; Schwarzinger, C.; Scharber, M. C.; Stadler, P. Anderson-Localization and the Mott-Ioffe-Regel Limit in Glassy-Metallic PEDOT. AEM **2017**, 3 (7), 1700050.
2. Farka, D.; Greunz, T.; Yumusak, C.; Cobet, C.; Mardare, C. C.; Stifter, D.; Hassel, A. W.; Scharber, M. C.; Sariciftci, N. S. Overcoming Intra-Molecular Repulsions in PEDTT by Sulphate Counter-Ion. Science and Technology of Advanced Materials **2021**, 22 (1), 985–997. https://doi.org/10.1080/14686996.2021.1961311.
3. Farka, D.; Kříž, K.; Fanfrlík, J. Strategies for the Design of PEDOT Analogues Unraveled: The Use of Chalcogen Bonds and σ-Holes. J. Phys. Chem. A **2023**, 127 (17), 3779–3787. https://doi.org/10.1021/acs.jpca.2c08965.
4. Farka, D.; Moreda, O. I.; Greunz, T.; Kříž, K.; Leeb, E.; Ulbricht, C.; Duchoslav, J.; Vacek, J.; Fanfrlík, J.; Yumusak, C.; Drnec, J.; Krajcovic, J.; Stifter, D.; Sariciftci, N. S. Polythieno[3,4-b]Pyrazine: Pathways to Metallic Charge-Transport. J. Mater. Chem. A **2025**. https://doi.org/10.1039/d5ta01145k.
5. Farka, D.; Ciganek, M.; Veselý, D.; Kalina, L.; Krajčovič, J. Epitaxial Guidance of Adamantyl-Substituted Polythiophenes by Self-Assembled Monolayers. ACS Omega **2024**, 9, 38733–38742. https://doi.org/10.1021/acsomega.4c04616.

L8

POLYMORPHS OF $Zn_xCu_{4-x}(OH)_6Cl_2$ AND THEIR PHYSICAL PROPERTIES

P. Doležal[1,2], V. Starosta[1], C. Krellner[3], P. Puphal[4], A. Pustogow[2]

[1]*Department of Condensed Matter Physics, Charles University, Czech Republic*
[2]*Institute of Solid State Physics, TU Wien, Austria*
[3]*Physikalisches Institut, Goethe-Universität Frankfurt, Germany*
[4]*Max Planck Institute for Solid State Research, Stuttgart, Germany*
petr.dolezal@matfyz.cuni.cz

Quantum spin liquid (QSL) is a theoretical model of spins with antiferromagnetic interactions. These spins fluctuate down to the absolute zero temperature without any long-range magnetic order but exhibit quantum entanglement [1]. A key aspect for realization of such theoretical concept is a geometrical frustration of these spins. In theory various QSL states have been identified, but much harder is to find a material, where this concept can be tested. Today only few materials are considered as QSL candidates. One of them is the mineral herbertsmithite, $ZnCu_3(OH)_6Cl_2$ [2]. The Cu^{2+} (S = 1/2) ions in this compound form a quasi-2D layered structure with kagome lattice [3]. Such a lattice exhibits high degree of frustration which is ideal for QSL. The rhombohedral crystal lattice (ideal kagome lattice) is stabilized by the Zn ions. The mineral clinoatacamite without Zn ions, $Cu_4(OH)_6Cl_2$, is then monoclinic and consequently antiferromagnetic order is stabilized at low temperatures [4]. The investigation of the ground state properties in the Zn-substituted series, $Zn_xCu_{4-x}(OH)_6Cl_2$, has therefore motivated numerous studies over the past two decades, usually on powder samples. In addition to their intriguing magnetic properties these compounds are also interesting from structural point of view. It is demonstrated by high amount of structural polymorphs. The presented study of single-crystalline samples is focused on the relation among these polymorphs and their ground-state properties, studied by low-temperature X-ray diffraction and specific heat measurements.

1. L. Balents, Nature, **464**, (2010), 7286.
2. M. R. Norman, Rev. Mod. Phys., **88**, (2016) 041002.
3. S. W. Braithwaite, R., Mereiter, K., Paar, W., Clark, A., Mineral. Mag., **68**, (2004), 527-539.
4. S.-H. Lee, H. Kikuchi, Y. Qiu, B. Lake, Q. Huang, K. Habicht, K. Kiefer, Nat. Mater., **6**, (2007), 853-857.

This work was supported by the Czech Science Foundation via research project GAČR 23-06810O.

L9

DIFFUSE SCATTERING IN (K,Na)NbO_3 SOLID SOLUTIONS

J. E. Flores Gonzales[1,2], N. Zhang[3], Z. An[3], M. Paściak[1]

[1]FZU - Institute of Physics of the Czech Academy of Sciences, Czech Republic
[2]Faculty of Mathematics and Physics, Charles University, Czech Republic
[3]Electronic Materials Research Laboratory, Key Laboratory of the Ministry of Education & International Center for Dielectric Research, School of Electronic Science and Engineering, Xi'an Jiaotong University, Xi'an, China.
floresgon@fzu.cz

In $KNbO_3$, the spontaneous polarization originates from displacements of Nb ions relative to the surrounding oxygen octahedra. In the rhombohedral phase, all Nb displacements are aligned along the same [111] direction, whereas in higher-symmetry phases this alignment becomes progressively less restricted due to a stepwise increase in the number of allowed Nb-displacement directions along ⟨111⟩. The orthorhombic phase allows two equivalent directions, the tetragonal phase four, and the cubic phase eight. This progressive increase in allowed displacement orientations introduces correlated disorder manifested by the stepwise appearance of diffuse scattering sheets in reciprocal space, evolving from (010) in the rhombohedral phase, to (010) and (100) in the tetragonal phase, and finally to {001} in the cubic phase [1].

(K,Na)NbO_3 solid solutions (KNN) are one of the leading Pb-free substitutes for (Pb,Zr)TiO_3 (PZT) with tunable piezoelectric coefficients [2]. Studies show the existence of a polymorphic phase boundary that might lead to extremely increased piezoelectric coefficients [3]. While it is accepted that the chemical disorder has a decisive role in producing this enhanced behavior, the exact short-range structure-property mechanisms are not well understood.

In this work we are interested in how addition of $NaNbO_3$ is affecting the correlation structure across the phase transitions. In particular, it is known that pure sodium niobate displays a complex behavior with at least six phase transitions between the high-temperature cubic phase and low-temperature rhombohedral one [4]. Some of the intermediate phases are incommensurate reflecting a complex interplay between polar order parameter and octahedral tilting. Tracking the changes in the single-crystal diffuse scattering we should be able to assess to which extent this interplay is also present in KNN with Na content ≤ 50 %.

1. R. Comes, M. Lambert, and A. Guinier, Solid State Commun. 6, 715 (1968).
2. X. Gao, Z. Cheng, Z. Chen, et al., Nat. Commun. 12, 881 (2021).
3. J. Fu and R. Zuo, Acta Mater. 195, 446 (2020).
4. E. Ringgaard and T. Wurlitzer, J. Eur. Ceram. Soc. 25, 2701 (2005).

Session III, September 9, Tuesday

L10

Data and what to do with it
DATA A CO S NIMI

Stanislav Daniš

Matematicko-fyzikální fakulta, Univerzita Karlova, Ke Karlovu 5, 121 16 Praha 2

Umělá inteligence (AI) rozproudila od svého vzniku řadu diskusí na témata "k čemu mi to bude?" až po otázky etického charakteru. Její přítomnost rozhodně změnila způsob vědecké práce. Avšak již dříve se používaly "učící se algoritmy", příchod AI jejich uplatnění podstatně zrychlil. V přednášce ukážeme několik uplatnění "chytrých algoritmů" ve výzkumu kondenzovaných látek publikovaných v časopisech Nature a Science. Naleznou své místo i v oblasti rozptylu rtg záření?

L11

NUCLEAR MAGNETIC RESONANCE IN SOLIDS

Vojtěch Chlan

Faculty of Mathematics and Physics, Charles University, Prague

Nuclear Magnetic Resonance (NMR) provides unique information on the local structure and dynamics of condensed matter and serves as a versatile technique in physics and material science, as well as a valuable tool in chemistry, biochemistry, molecular biology, and medicine. Solid-state NMR spectroscopy allows investigation of a wide range of materials, including crystalline and disordered solids, with unique capabilities for probing both structural and magnetic properties. Local crystal symmetry, valence state. In magnetic solids, though often challenging, NMR spectroscopy yields additional information about the magnetic state of atoms, can study individual magnetic sublattices, or reveal the direction of magnetic moments.

In the talk, the basic principle of NMR and related spectroscopy will be introduced, its application to solids and magnetic solids will be covered – with a focus on areas where NMR spectroscopy can serve as a complementary method to diffraction techniques.

.

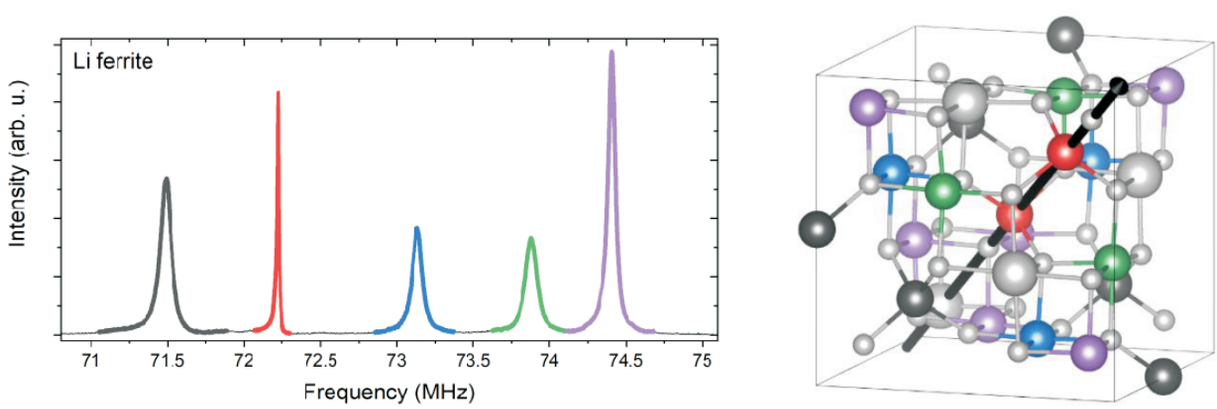

Figure 1. ^{57}Fe NMR spectrum of ferrimagnetic Li spinel ferrite with individual Fe sites distinguished in the unit cell. Five spectral lines appear both because of crystallographic and magnetic non-equivalence of Fe atoms.

L12

SELECTED EXAMPLES IN X-RAY REFLECTOMETRY

Lukáš Horák

Charles University, Faculty of Mathematics and Physics, Prague, Czech Republic
lukas.horak@matfyz.cuni.cz

X-ray reflectivity (XRR) is a well-established and, in principle, straightforward technique for determining the depth profile of electron density in thin films [1]. The presence of interference fringes (Kiessig fringes) in the reflectivity curve typically allows for a direct and accurate estimation of layer thickness. However, in many practical cases, these fringes are weak, distorted, or even completely absent (Figure 1); yet meaningful structural information can still be extracted.

Even when sample imperfections such as surface curvature or thickness inhomogeneity suppress or smear the interference fringes, the absorption contrast can still be exploited to reliably estimate the average layer thickness.

For each sample, one must carefully consider the appropriate level of model complexity for data fitting. Should the model be kept as simple as possible, even if it fails to adequately reproduce the measured data? In cases where the fit is as poor as for some samples shown in Figure 2, how trustworthy are the extracted parameters? Furthermore, is it feasible to fit the electron density depth-profile directly, and if so, can such an approach yield a unique and physically meaningful solution?

This presentation will explore several such cases, where the absence of clear fringes or the use of oversimplified models did not prevent the retrieval of reliable density profiles. Surprisingly, even models that poorly fit the experimental data can yield results comparable to those obtained using significantly more complex and computationally demanding approaches. This raises important questions about the trade-off between model fidelity and interpretability, especially in the context of peer review and publication.

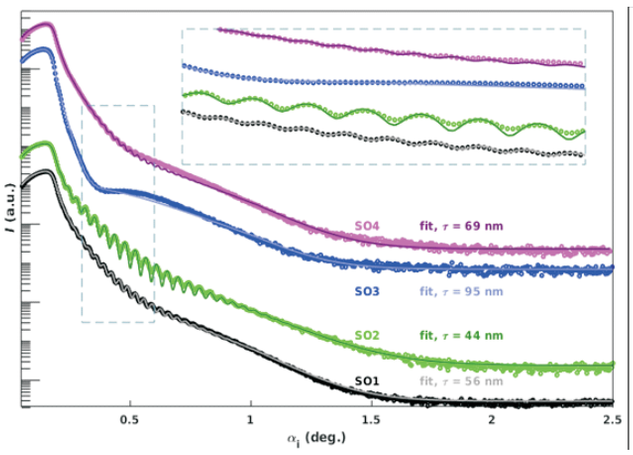

Figure 1. XRR curves measured on Hydrogenated U layers. As it is visible in the inset with the zoomed part, no thickness fringes are present for the sample SO_3. Is it still possible to determine/estimate the layer thickness by XRR?

1. L. G. Parratt, *Phys. Rev.* **95**, 359–369 (1954). DOI: 10.1103/PhysRev.95.359.

The work was supported by the project GA ČR, reg. No. 24-12710S.

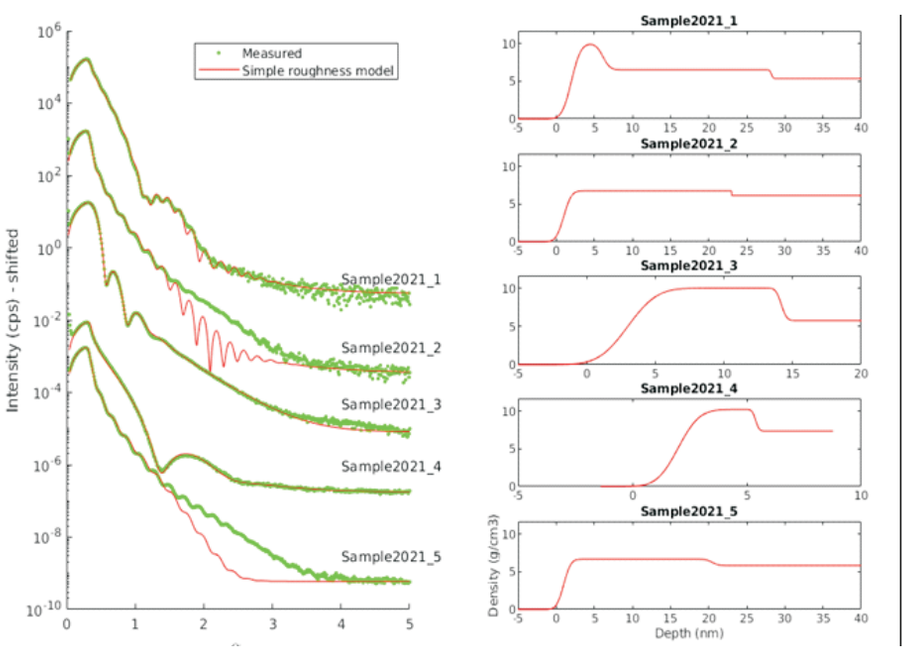

Figure 2. (left) XRR curves of BIO/DTO bilayers on YSZ substrate fitted by the most simple model of two layers with rough interfaces; (right) density depth-profiles visualized for the refined parameters of the model. How reliable are the fitting results when the experimental data are evidently not fully fitted?

Session IV, September 9, Tuesday

L13

First experience with single crystal diffractometer Synergy Rs

PRVNÍ ZKUŠENOSTI S MONOKRYSTALOVÝM DIFRAKTOMETREM SYNERGY VYBAVENÝM ROTAČNÍ ANODOU A ZAKŘIVENÝM HYBRIDNĚ PIXELOVÝM DETEKTOREM

M. Dušek, V. Petříček

Institute of Physics of the Czech Academy of Sciences, Na Slovance 2, 182 21 Praha 8, Czech Republic
dusek@fzu.cz

Nový monokrystalový difraktometr s rotační anodou a velkým zakřiveným detektorem od firmy Rigaku Oxford Diffraction je ve Fyzikálním ústavu v provozu od března 2025. Důvodem nákupu byla potřeba doplnit stávající, zcela přetížený, difraktometr SuperNova přístrojem, který by dosahoval řádově vyšší intenzity při zachování podobného průměru primárního svazku. Průměr svazku je v podmínkách naší laboratoře důležitým parametrem vzhledem k častým experimentům s vysoce adsorbujícími krystaly. Přístroj je navíc vybaven programově ovladatelnou divergenční clonou a možností nastavit energetické okénko pro potlačení luminiscence.

Po několika měsících trvalého provozu jsme dosáhli efektu, který se projevil u všech dříve zakoupených difraktometrů: od počátečního zděšení, co si počneme s tolika výsledky, jsme opět v situaci, kdy typické měření jednoho vzorku trvá jeden až dva dny. Rozdíl je pouze v tom, že dříve bychom tyto vzorky vyřadili jako neměřitelné. V čem je tedy skutečné zlepšení, když pomineme výhodu pro chemiky, kteří mohou stále víc odbývat přípravu kvalitních monokrystalů? V přednášce ukazujeme, že skutečné zlepšení spočívá v tom, že z krystalu dobré kvality můžeme vydobýt podstatně víc informací.

Jako příklad jsme použili krystal YP_3O_9, jehož struktura byla publikována v roce 2003 [1] jako standartní struktura. Později byla látka změřena jako (3+1)d modulovaná, tedy s jedním modulačním vektorem, a dlouhá léta používána v tzv. Kuchařce programu Jana2020 [2] jako příklad jednoduché modulované struktury. Ve finální řešení ale pro některé řezy superprostorem vycházely nesmyslné „teplotní“ parametry (ADP – atomic displacement parameters), což nás vedlo k přeměření vzorku na

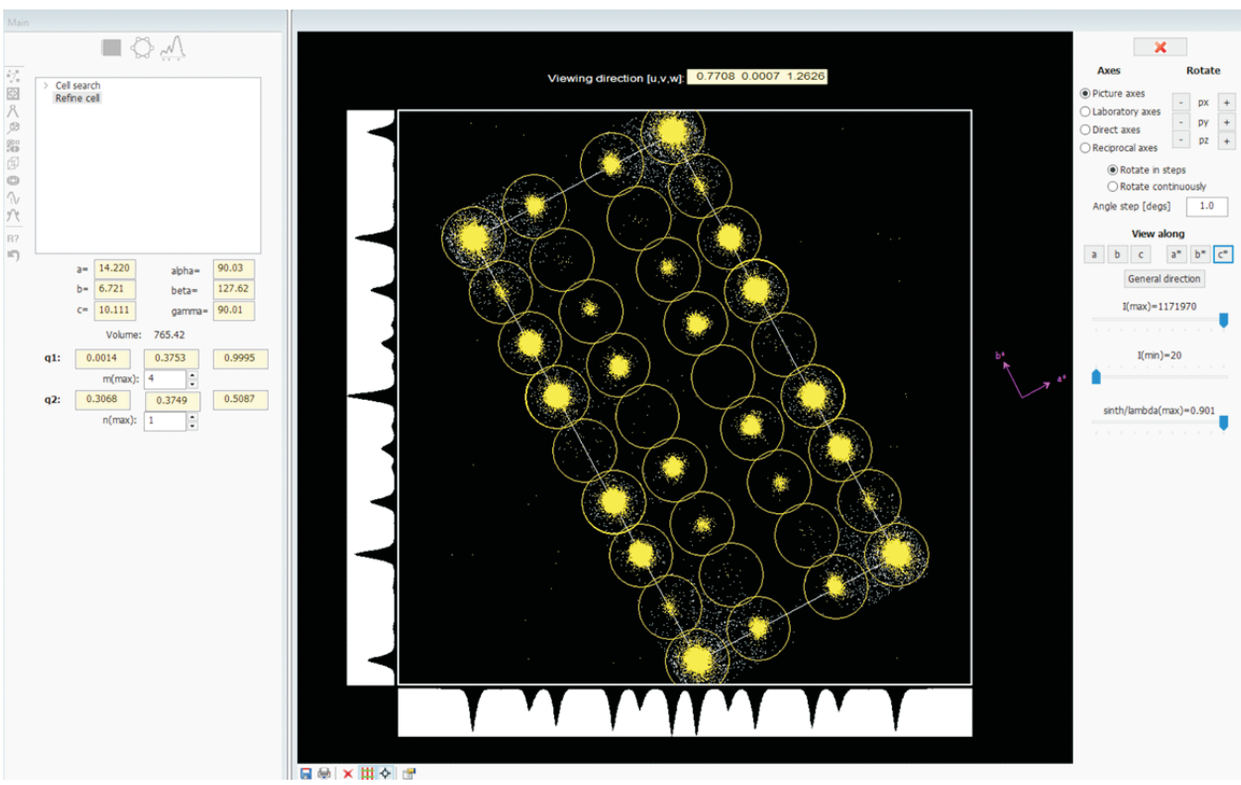

Obrázek 1. Indexační nástroj programu Jana2020 ukazující projekci nahledaných píků do jedné základní buňky. Na delší hraně zobrazené buňky vidíme první, druhé a třetí satelity popsané q-vektorem (0, 0.375,0). Nejintenzivnější reflexe uvnitř buňky jsou první satelity popsané q-vektorem (0.307, 0.375, 0.509). Všechny ostatní stopy lze popsat kombinací obou q-vektorů, čímž je indexován celý difrakční obraz (cca 98% nahledaných píků).

difraktometru Supernova. Zde se ukázalo, že existuje další set mnohem slabších satelitních reflexí, a že tedy strukturu lze popsat pouze s dvěma modulačními vektory. Data ale byla příliš slabá, než aby to stálo za vynaložené úsilí. Konečně, v tomto roce, byl ten samý krystal přeměřen na našem novém difraktometru. Několikadenní měření ukázalo, že kromě druhého modulačního vektoru existují i satelitní reflexe vzniklé kombinací obou modulačních vektorů, což je důkazem, že se jedná o (3+2)d modulovanou strukturu. Získaný difrakční obraz ukazuje obr. 1.

Difraktometr s takto intenzivním zdrojem vrací do hry starou otázku, jestli je lepší měřit vzorek deset minut na synchrotronu, anebo týden v domácí laboratoři. Naše zkušenosti ukazují, že pokud nemáme dlouholeté zkušenosti se synchrotronovým experimentem a dobré kontakty na tamější experimentátory, je lepší věnovat na to experimentální čas a měřit doma.

V závěru přednášky ukážeme, jakou strategii sdílejí výrobci difraktometrů a výrobci mikrovlnných trub a rychlovarných konvic.

1. M. Graia, A. Driss, T. Jouini, *Solid State Sciences,* **5**, (2003), 393.
2. V. Petříček, L. Palatinus, J. Plášil, M. Dušek, , *Z. Kristallog. – Cryst. Mater.*, **238**, (2023), 271.

L14

INTERPRETATION OF ELECTRON DENSITY MAPS USING NEURAL NETWORKS

Jiří Zelenka, Jan Rohlíček

Institute of Physics of the Czech Academy of Sciences, Prague

The interpretation of Fourier maps is an important process in X-ray diffraction analysis. Their quality and resolution can be limited by a number of factors, including the disorder of atoms in the crystal and poorly measured diffraction data, which can be caused, for example, by crystal instability during the experiment, twinning, small crystal size, or otherwise poor quality of the measured crystals. These imperfections often lead to blurred or difficult-to-interpret maps, which complicate the determination of the crystal structure and cause headaches for many crystallographers.

In this work, we present a possible approach that could help interpret low-resolution maps. This approach uses deep learning capabilities to recognize and reconstruct relevant features in maps. In the reconstructed maps, noise is removed and blurred parts of the map, which appear to be meaningless blobs, are interpreted. This approach can be applied at various stages of structural analysis. For example, when interpreting maps after solving a phase problem or interpreting differential Fourier maps. This approach is also applicable to various groups of substances and materials, regardless of whether they are inorganic, organic, or even protein structures, thus opening up new possibilities for streamlining the entire structural analysis process.

L15

USE OF INTERMOLECULAR DISTANCES IN SOLVING STRUCTURES FROM POWDERS

J. Rohlíček[1], J. Brus[2], V. Eigner[3]

[1]*Institute of Physics of the Czech Academy of Sciences, Na Slovance 2, Prague 8, 182 21, Czech Republic*
[2]*Institute of Macromolecular Chemistry, Czech Academy of Sciences, Heyrovsky Square 2, Prague, 16206, Czech Republic*
[3]*Department of Solid State Chemistry, University of Chemical Technology Prague, Prague 6, 166 28, Czech Republic*
rohlicek@fzu.cz

This study introduces a methodology that incorporates supplementary structural information about intermolecular distances obtained from solid-state NMR (ssNMR) measurements into direct-space approach for crystal structure determination from powder diffraction (PD) data [1]. In these methods, such intermolecular distances are applied as restraints within the global optimization process. Direct-space techniques are highly effective for solving structures from PD data, particularly when only a laboratory diffractometer is available. They employ global optimization algorithms which, iteratively test candidate structural models for agreement with experimental diffraction patterns.

For structurally simple, well-diffracting compounds, the probability of identifying the correct model is high. However, the success rate decreases rapidly with the number of degrees of freedom (DOF). A compound with six DOF can often be solved within seconds, whereas those with around 40 DOF are frequently unsolvable using PD data alone, except in rare cases [2]. The problem becomes even worst for poorly crystalline materials, where peak broadening reduces the resolution of diffraction data.

In this work, selected intermolecular distances determined from ssNMR experiments were used as additional restraints in the structure determination process. The FOX software [3] was modified to include a new term in the cost function that enforces agreement with experimentally derived interatomic distances between specific atoms of different molecules. These restraints, assigned tolerances based on NMR measurement precision, were tested on a series of relatively simple isothiouronium salts. To simulate challenging experimental conditions, diffraction peak profiles were artificially broadened. The results demonstrate that including ssNMR-based restraints significantly improves the likelihood of obtaining the correct structural solution, even from low-quality PD data.

1. J. Rohlíček, V. Eigner, J. Czernek, J. Brus, *J. Appl. Crystallogr.* **58** (2025) 321-332.
2 M. Husak, A. Jegorov, J. Czernek, J. Rohlicek, S. Zizkova, P. Vraspir, P. Kolesa, A. Fitch, J. Brus, Cryst. Growth Des. 19 (2019) 4625-4631.
3. V. Favre-Nicolin, R. Černý, Z. Für Krist. - Cryst. Mater. 219 (2004) 847-856.

This work was supported by the Grant Agency of the Czech Republic, project no. 23-05293S.

Session V, September 9, Tuesday

L16

PROTEIN CRYSTALLIZATION

J. Hašek

Institute of Biotechnology, Czech Academy of Sciences, Průmyslová 595, Vestec,252 50
hasekjh@seznam.cz

Introduction

Protein crystallization has been used for decades for structure determination of detailed molecular structure of proteins in atomic resolution. Millions of successfully performed crystallization experiments by the trial and error method have shown that the presence of other substances is practically always necessary for the regular ordering of protein molecules into the crystal. The very laborious development of crystallization screens has led to the massive deployment of large crystallization robots that control the precise setting of the composition and the change of the chemical parameters. Currently, the successful crystallization is expected in about one quarter of new proteins.

However, the fundamental problem is that almost everything is based on practical experience and there is no trustful and logical explanation of the principle on which crystallization agents work. Neither is clear when to use which crystallization agents nor whether it is appropriate to combine them with each other.

Dynamic Theory of Protein Crystallization

Our Dynamic Theory of Protein Crystallization (DTPC) hopefully explains all the uncountable crystallization experiments that have been described during the last decades of experience with protein crystallization [1].

A practice of the last decades clearly showed that the successful protein crystallization requires a presence of additives directly influencing regular stacking of protein molecules in the crystal. We call them **Protein Crystallization agents (PCA).** By definition these special crystallization additives control amounts of miss-placed and miss-oriented molecules in the growing solid. Thus, they practically control the difference between the crystalline and amorphous solid state. Do not misinterpret them with another crystallization additives added for different reasons. Imagine also that some chemicals can play several important roles in the crystallization solution.

Another important point is that the protein in the oversaturated crystalline solution are highly influenced by the specially added PCA. It is well proved that in the molecularly overcrowded crystallization solution, there is high concentration of **temporary protein-PCA adducts (P-PCA adducts).** Properties of the adhesion patches on protein surface and also the orientation of the P-PCA adduct with respect to its motion in solution will change significantly in comparison with the naked protein. Non-covalent bonds between protein and PCA should be weak to allow fluent release of PCA molecules from the growing crystal back to solution.

It is obvious that very large surface of protein molecules always has many adhesion patches that compete with each other when depositing the protein molecule into the crystal. It is also evident, that if protein join to the crystal surface in an incorrect way, it will definitely stay as a stacking fault. It is improbable, that the molecule will dissolve again, turns to the correct orientation and join the surface again. Thus, the classical thermodynamics is not sufficient. The physical laws of rigid body motion in liquids play an important role here.

This presentation will show some examples of how the experimenter influences the way in which protein molecules stack in the growing crystal and also how the crystal seeds grow from the beginnings.

We will show the function on examples of experimentally best confirmed crystallization agents :

- how the experimenter influences the kinetics of molecules, the correct orientation and the position of the protein molecules depositing on the surface of the growing crystal,
- how low-molecular crystallization agents work (for example malonates [2]),
- how high-molecular crystallization agents work (for example polyethylene glycol (PEG-2000) [3]),
- on what principle artificial and natural porous crystallization catalysts work.

In the Appendix, there is a list of definitions useful in the Dynamic Theory of Protein Crystallization (DTPC).

The work was supported by the Czech Science Foundation 25-17546S.

1. Hašek, J., (2011) *Principle of the unique adhesion mode in protein crystallization*, Acta Cryst. A67, C537;
2. McPherson, A. (2001) *Comparison of salts for the crystallization of macromolecules*, Protein Science, 10418-10422.
3. Kimber,M.S. et al, (2003) *Crystal screen optimization. Data mining crystallization databases: Knowledge-based approaches to optimize protein crystal screens,* Proteins, 51, 562-568.

Appendix

Definition of terms – Glossary

Glossary summarizing some terms important for the dynamic theory of protein crystallization and their abbreviations used in this work

Aditives Different compounds utilized for preparation of crystallization solution called additives. Some additives have more functions in the crystallization solution. Their reported purposes are:

- to control stacking the protein molecules in the growing crystal
- to increase solubility of the protein, prevent its aggregation,
- to control nucleation,
- to modulate crystal habit,
- to optimize buffer conditions,
- to modulate pH and ionic strength,
- to stabilize the protein,
- to protect denaturation
- to protect formation of ice during flesh freezing
- to control of viscosity of solution to slow down flows and diffusion, etc.

PCA

Protein c**rystallization agents** directly influencing the stacking of protein molecules in the growing crystalline phase

VA

Viscosity agents - added to increase viscosity of the solution to slow diffusion

Protein-PCA aduct

Protein molecule temporarily linked to (non-covalently clustered) the molecules of protein crystallization agents (PCA)

Precipitant

Precipitation agents – the compound with high affinity to water molecules reducing thus amount of free water molecules in solution

CTPC

Classical theory of protein crystallization considers crystal growth as a regular sedimentation of ideally dissolved (uncomplexed) protein molecules into the crystalline phase in some pre-defined environment. A regular stacking of protein molecules is derived from thermodynamic parameters.

DTPC

Dynamic theory of protein crystallization takes into account formation of temporary molecular aggregates in the crystallization solution. The activities of the temporary aggregates are important particularly during the crystal initiation phase. **It** recognizes the non-equilibrium nature of protein crystallization and analyses the kinetics of intermediate states during crystallization process and explains why the correct setting of the crystallization experiment leads to regular crystals instead of irregular sediment during the solidification process..

Direct observations of the temporary nano-scaled molecular processes in the highly concentrated solutions are usually difficult. The proof of intermediate processes is validated usually by indirect macroscopic observations.

AP

Adhesive patch is the region on the surface of a protein molecule responsible for adhesion to the adjacent molecule. Protein have usually many adhesive patches on its surface – but, only some of them can form intermolecular contacts in a given configuration of molecules in the solid state.

PPAM

Protein-protein adhesion mode. It is an abstract term describing a tendency to some specific adhesion between two or more protein molecules. It does not describe an exact geometry of the molecular adduct. The particular spatial realization of the contacts depends always on the molecular environment (the composition of the crystallization solution, the phase, etc.). It means that the complementary patches on surfaces of the adhering proteins differ in different environments. Despite these differences, it is usually easy to identify any particular adhesion mode in different molecular environments such as dilute solution, concentrated solution, amorphous, crystalline phase, in living tissue, etc.

DAM

Dominant adhesion mode is the PPAM leading to the highest decrease of free energy of system in a given environment. It depends on the molecular environment and thus can be changed by experimenter, e.g. by composition of crystallization solution. Thus, DAM is not a property of a given protein compound only. It can be changed by experimenter.

PDAM

Principle of the Dominant Adhesion Mode. It is the evident principle saying that only one PPAM must dominate crystallization to get a regular crystalline phase. It must be respected by any crystallization method.

SAM

Subsidiary adhesion modes are the PPAM compatible with the dominant DAM in a given space group. The free energies of the DAM and SAMs are decisive for the crystallization rates in the respective crystal directions.

IAM

Incompatible adhesion mode. The protein-protein adhesion mode (PPAM) which is incompatible (cannot coexist) with the dominant adhesion mode (DAM) in a given crystalline form.

MPPI

Modulators of Protein-Protein Interaction. The compounds temporarily modifying the adhesion properties between the target protein molecules. There are several important subclasses of these compounds described bellow.

PSAM

Protein Surface Active Molecules. The molecules forming temporary adducts with the target protein molecules and changing thus the adhesive properties of the protein-PSAM adduct envelope with respect to the envelope of the naked protein. Temporary covering the specific patches on the protein surface influences the stacking of protein molecules into the growing crystal. Many efficient PSAMs are already used in crystallization experiments as precipitants or as additives.

PSSA
Protein Surface Shielding agents the molecules designed to bind the protein surface patches important for crystallization in an unwanted crystal form.
PPLM
Protein-Protein Linking Molecules are the molecules designed to bind surfaces of two protein molecules forming thus a temporary molecular adduct in solution. The PPLM molecules are sometimes observed in structures deposited in the PDB.
CSAM
Compatible Set of Adhesion Modes. The set of cooperative adhesion modes which are mutually compatible within a given crystal form.
PXAM
Protein-PSAM Adhesion Mode. Due to the large variability of protein surface, small molecules have usually many adhesion patches on the protein surface.
TPA
Temporary protein adducts are semi-stable complexes of the protein molecules with some other molecules. If the adducts are stable enough, the adjoining molecules can effectively block an access to some areas on the surface of the target protein molecule.

Initiation of protein crystallization

CI Crystallization initiator (catalyst) is a heterogeneous object inducing protein crystallization. It acts as a catalyst for the formation of stable and regular crystal nuclei. Stable nuclei can separate and continue to grow far from the surface of the CI.
PIC
Porous initiator of crystallization is the CI, where its morphology has dominant effect on crystallization.
CN
Crystallization nucleus (crystal seed) is a crystalline aggregate of molecules that has potential to grow under suitable conditions into a stable crystal.
Substrate
is material used to prepare the CI. It need not show any nucleation properties itself.
Nucleant
is a particle or some specific surface element that triggers the nucleation of the target material.
MIP
Molecularly imprinted polymer – polymer with preformated cavities imprinted by some molecular objects.
Cognate MIP
The MIP imprinted by the target protein molecule.
NIP
Corresponding **Not Imprinted Polymer** as a negative evidence in the MIP activity tests.
CNM
Carbon Nano-Material is characterized by a large ratio surface to volume –– for example carbon nanotubes, or carbon “fractal” nanoparticles (e.g. carbon black).

Ordering in solution

Kosmotropic agents
the molecules or ions supporting ordering of the neighbor solvent molecules and stabilizing thus the protein structure. They support formation of well-ordered 3D sets of intermolecular interactions.
Chaotropic agents
the molecules or ions exerting chaotropic effect in solution and generally destabilizing protein conformation. Their presence brakes formation of a regular net of hydrogen bonds between water molecules in solution.
Malonates
the compounds forming malonate anion in solution ($^{-}OOC\text{-}CH_2\text{-}COO^{-}$)

Polymers

Polyether
Class of polymers with the repeating pattern R-O-R’. Smile notation ORORORO…ORO.
Crown ether
Cyclic oligomers of polyether with outstanding and tunable chelating ability to cations and to the hydrogen-bond-donor molecules.
PEG = Poly(ethyleneglycol) = poly(oxyethylene) = poly(ethyleneoxide) = macrogol.
Polymers with chemical formula $H\text{-}(O\text{-}CH_2\text{-}CH_2)_n\text{-}OH$ (Smile notation OCCOCCOCC…OCCO). High flexibility of the PEG chain allows formation of loops where the loan electron pairs of successive ether oxygens orient to the a single center binding thus selectively some cations. They act also as eficient hydrogen-bond-acceptors forming relatively stable adducts with hydrogen bond donor. PEG belongs also to the class of polyethers.
Database of protein-polymer interactions (DPPI)
set of protein structures selected from the PDB (Protein Data Bank), containing polymer fragments. It involves also the imaging tools allowing easy viewing and the serial analysis of intermolecular contacts of individual polymer fragments to the protein surface. It greatly simplifies analysis of the protein-PSAM adhesion modes.
LB films - Langmuir-Blodget films
Well-ordered films composed of monomolecular layers of macromolecules used by Pechcova and Nicollini for the preparation of protein crystal initiators.
PDMS - PolyDiMethylSiloxane
The polymer used by Ghatak *et al* for preparation of roughly waved surface by an incision of the stretched folies.
NHMA - N-hydroxymethylacrylamide
The polymer used as a matrix for molecular imprints by Saridakis *et al*.

L17

INFORMATION ON PROTONATON IN BIOMOLECULAR STRUCTURES

J. Dohnálek[1], K. Adámková[1], M. Trundová[1], B. Husťáková[1], J. Dušková[1], P. Kolenko[1,2], L. Gajdoš[3], T. Skálová[1], T. Kovaľ[1]

[1]*Institute of Biotechnology, Czech Academy of Sciences, Průmyslová 595, 25250 Vestec*
[2]*Czech Technical University in Prague, Břehová 7, 115 19, Prague*
[3]*Institut Laue-Langevin, 71 avenue des Martyrs, 38042 Grenoble*
dohnalek@ibt.cas.cz

Hydrogen plays a key role in structure and function of biomolecules. Intermolecular interactions rely amongst others on a finely tuned concert of hydrogen bonds formation and typical protonation patterns. Structural information on hydrogen/proton presence and localization in structural biology is not easily accessible.

S1-P1 nucleases are coded for by fungi, trypanosomatids, plants and some pathogenic bacteria [1]. The active site relies on the metal cluster (typically containing zinc) and the nucleobase-binding site 1 stabilizing the –1 nucleotide with respect to the cleaved O3'-P3' bond. The enzymes cleave DNA, RNA, single strands, double strands, viroids, some modified nucleotides, oligonucleotides and genomic DNA [1]. While their fold does not change across the species, their activity profiles differ dramatically.

Our structure-function studies of S1-P1 nucleases from plants, fungus, and two bacterium species [2-5], including crystal structures, mutagenesis, numerous product/ligand complexes helped us better understand the structure-function questions, such as active site remodelling and key mobility elements in the active site. In a recent study we have identified SmNuc1 from opportunistic pathogen *Stenotrophomonas maltophilia* with unusually high catalytic rates for this enzyme class. We could identify the key region for RNA/DNA preference and discovered its high activity towards cyclic-di-GMP, the bacterial second messenger [6]. Our crystallographic studies answered key questions regarding non-specificity of S1-P1 nucleases and brought us closer to understanding protonation details of the protein-nucleic acid interactions.

The excellent diffraction properties of S1 and SmNuc1 nuclease crystals enable atomic resolution studies with the promise of mapping of important protonation patterns with the use of neutron radiation and sub-Ångstrom resolution X-ray crystallography.

1. T. Koval, J. Dohnalek *Biotechnol. Adv.* (2017) Epub 2017 Dec 14, 10.1016/j.biotechadv.2017.12.007.
2. T. Kovaľ T, L.H. Østergaard, J. Lehmbeck, *et al. PLOS One* 11, (2016), e0168832.
3. M. Trundová, T. Kovaľ, R.J. Owens, *et al. Int J Biol Macromol* **114**, (2018), 776.
4. K. Adámková, T. Koval', L.H. Østergaard, *et al. Acta Crystallogr D***78,** (2022), 1194.
5. B. Husťáková, M. Trundová, K. Adámková, et al. *FEBS Lett* **597**, (2023), 2103.
6. K. Adámková, M. Trundová, T. Kovaľ, B. Husťáková, *et al. FEBS J.*, **292**, (2025), 129.

This work was supported by the Czech Science Foundation (25-17546S), and by the Czech Academy of Sciences (86652036). CIISB, Instruct-CZ Centre of Instruct-ERIC EU consortium, funded by MEYS CR infrastructure project LM2023042 and European Regional Development Fund-Project No. CZ.02.01.01/00/23_015/0008175 is acknowledged for providing access to all facilities at CMS in BIOCEV for this project.

L18

ADVANCES IN ANNOTATION AND VALIDATION OF NUCLEIC ACIDS

Bohdan Schneider, Lada Biedermannová, Paulína Božíková, Michal Malý, Terezie Prchalová, Jakub Svoboda & Jiří Černý

Institute of Biotechnology of the Czech Academy of Sciences, 252 50 Vestec, Czech Republic
bohdan.schneider@ibt.cas.cz

Structural biology operates robust tools and data for proteins; the field of nucleic acid (NA) structure analysis and prediction lags behind. This is serious for RNA structures in the context of the ability to predict their variable 3D structures and for DNA for understanding of their mutual recognition with proteins. More reliable prediction of RNA 3D structures is primarily hindered by a scarcity of sequence alignments of functionally wide spectrum of RNAs. A better understanding of both RNA and DNA could be much more profound if more high-quality structures were available, and the quality of the existing structures was gauged more reliably [1]. Our work addresses the latter, improving the quality of the existing NA structures and methods of their analysis. Current challenges in NA structure quality include: (A) Inconsistent application of valence geometry restraints. (B) Poorly refined backbone conformations. (C) Incomplete or incorrect base pairing assignments. This presentation will introduce key features of fully redesigned DNATCO version 5.0 at dnatco.datmos.org [2], a suite of web-based tools designed

to enhance NA structure annotation and validation. DNATCO includes:

An Annotation TAB for clear structural overviews. Quite significantly, the new DNATCO provides full annotation of base pairs in the Leontis-Westhof classification schema [3] both in tabular form and - to the best of our knowledge - for the first time as an integrated part of molecular graphics.

A Validation TAB offering detailed analysis, including dinucleotide conformation analysis (based on our NtC classification [4]), novel RMSD/RSCC scatterplots, and detailed valence geometry evaluation.

A Browse TAB for multi-view structure visualization.

Our ongoing development aims to provide tools for direct structure modification during the refinement process, further contributing to higher-quality NA structural data.

1. Schneider, B., Sweeney, B.A., Bateman, A., Cerny, J., Zok, T. and Szachniuk, M. (2023). When will RNA get its AlphaFold moment? *Nucleic Acids Res*, **51**, 9522-9532.

2. Jiří Černý, Michal Malý, Paulína Božíková, Terezie Prchalová, Jakub Svoboda, Lada Biedermannová & Bohdan Schneider: DNATCO v5.0: Integrated Web Platform for 3D Nucleic Acid Structure Analysis. submitted to *Nucleic Acids Research* (2025).

3. Leontis, N.B. and Westhof, E. (2001) Geometric nomenclature and classification of RNA base pairs. *RNA*, **7**, 499-512.

4. Jiří Černý, Paulína Božíková, Jakub Svoboda & Bohdan Schneider: A unified dinucleotide alphabet describing both RNA and DNA structures. *Nucleic Acids Research*. **48**: 6367-6381 (2020). doi: 10.1093/nar/gkaa383.

This research was funded by Czech Academy of Sciences, grant RVO 86652036 and by grant LM2023055 to ELIXIR CZ from MEYS Czech Republic.

L19

CRYSTAL STRUCTURE OF BLUE LACCASE BP76, A UNIQUE TERMITE SUICIDAL DEFENSE WEAPON

Jiří Brynda[1], Jana Škerlová[1], Jan Šobotník[2,3], Marek Zákopčaník[4], Petr Novák[4], Thomas Bourguignon[5], David Sillam-Dusses[6] & Pavlína Řezáčová[1]

[1]Institute of Organic Chemistry and Biochemistry, Czech Academy of Sciences, Prague, 160 00, Czech Republic
[2]Faculty of Tropical AgriSciences, Czech University of Life Sciences, Prague, 165 00, Czech Republic
[3]Institute of Entomology, Biology Centre, Czech Academy of Sciences, České Budějovice, 370 05, Czech Republic
[4]Institute of Microbiology, Czech Academy of Sciences, Prague, 142 20, Czech Republic
[5]Okinawa Institute of Science and Technology Graduate University, Okinawa, 904-0495, Japan
[6]Laboratory of Experimental and Comparative Ethology, UR 4443, Université Sorbonne Paris Nord, Villetaneuse, 93430, France
rezacova@uochb.cas.cz

Aging workers of the termite *Neocapritermes taracua* can defend their colony by sacrificing themselves by body rupture, mixing the externally stored blue laccase BP76 with hydroquinones to produce a sticky liquid rich in toxic benzoquinones. Here, we describe the crystal structure of BP76 isolated from *N. taracua* in its native form (Figure 1) [1]. The structure reveals several stabilization strategies, including compact folding, glycosylation, and flexible loops with disulfide bridges and tight dimer interface. The remarkable stability of BP76 maintains its catalytic activity in solid state during the lifespan of *N. taracua* workers, providing old workers with an efficient defensive weapon to protect their colony.

1. Skerlova, J. *et al*. 2024. Structure 32, 1-5. https://doi.org/10.1016/j.str.2024.07.015

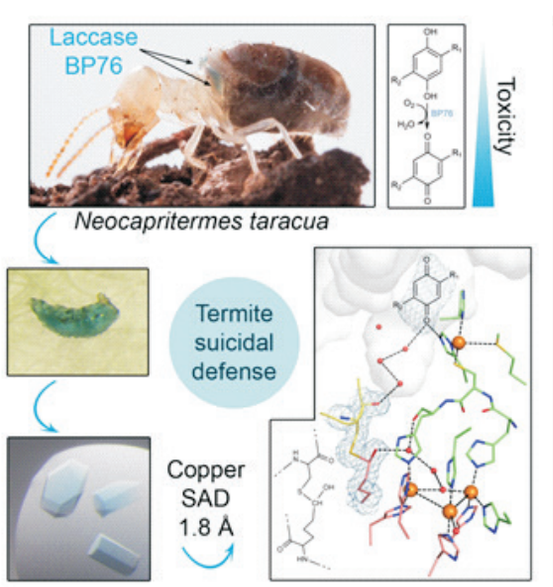

Figure 1. Crystal structure of blue laccase BP76 from *Neocapritermes taracua*.

Session VI, September 9, Tuesday

L20

PROTEIN ENGINEERING OF INTERLEUKIN 24 TARGETING HIGHER THERMAL STABILITY AND STRUCTURE:FUNCTION STUDIES

P. Kolenko[1,2], L. Kolářová[2], Y. Peleg[3], B. Schneider[2], J. Zahradník[4]

[1]Czech Technical University in Prague, Břehová 7, Prague 115 19, Czechia
[2]Institute of Biotechnology, Czech Academy of Sciences, Průmyslová 595, 252 50 Vestec, Czechia
[3]Weizmann Institute of Science, Rehovot, Israel
[4]1st Faculty of Medicine, Charles University, BIOCEV, Prague 252 50, Czechia
kolenpe1@cvut.cz

Evolution has optimized protein variants with respect to the life of an organism in its surroundings. For example, protein variants in bacteria living in high temperatures have usually higher thermal stability than those of bacteria living in arctic environments. Higher thermal stability is frequently required in biotechnologies as this usually goes hand in hand with increased stability in various denaturing agents, natural environment, and with higher expression yields.

Human interleukin 24 has a potential in treatment for autoimmune diseases and cancer [1]. It is a relatively instable protein, and its expression usually provides low yields. We designed optimized variants using the PROSS algorithm [2], performed various biophysical and function studies, and successfully crystallized more stable variant having 30 point mutations (~ 20 % of all amino acids). We determined the crystal structure at 1.3-Å resolution.

Unfortunately, this protein variant lost some of its functions that are related to binding its biological interaction partners IL-20R1 and IL-22R1. However, the function was restored to 80 % of its wild-type variant with a single reverse mutation to the wild-type residue Thr198. Such protein variant can be used for further optimization and subsequent application in clinical studies.

1. J. Zahradník, L. Kolářová, Y. Peleg, P. Kolenko, S. Svidenská, T. Charnavets, T. Unger, J.L. Sussman, B. Schneider, *FEBS Journal*, **286**, (2019), 3858-3873.
2. A. Goldenyweig, M. Goldsmith, S.E. Hill, O. Gertman, P. Laurino, Z Ashani, O. Dym, T. Unger, S. Albeck, J. Prilusky, R.L. Lieberman, A. Aharoni, I. Silman, J.L. Sussman, D.S. Tawfik, S.J. Fleishman, *Mol. Cell*, **63**, (2016), 337-346.

L21

CHARACTERIZATION OF PROTAC-580: A CEREBLON-RECRUITING DEGRADER OF ENTEROVIRAL 2A PROTEASE

B. Kaščáková[1], H. Durmaz[3], R. Kumar Akula[3], K. Rox[3], H. El Kilani[2], R. Hilgenfeld[2] and I. Kutá Smatanová[1]

[1]Department of Chemistry, University of South Bohemia, Branišovská 1645/31a, 370 05 Ceske Budejovice, Czech Republic
[2]Institute for Molecular Medicine, University of Lübeck, Ratzeburger Allee 160, 23538 Lübeck, Germany
[3]Department of Chemical Biology, Helmholtz Centre for Infection Research, Inhoffenstr. 7, Braunschweig 38124, Germany
karafb00@jcu.cz

Enteroviruses (EV) such as EV-A71 and EV-D68 are increasingly recognized as serious public health threats, particularly among children [1], due to their association with severe neurological and respiratory illnesses including hand, foot, and mouth disease (HFMD) [2] and acute flaccid myelitis (AFM) [3]. Despite their impact, no targeted antiviral therapies are currently available. To address this gap, we have developed PROTAC-580, a first-in-class cereblon-recruiting proteolysis-targeting chimera (PROTAC) designed to degrade the enteroviral 2A protease ($2A^{pro}$), a viral enzyme essential for replication and immune evasion.

$2A^{pro}$ mediates polyprotein processing, inhibits host protein synthesis via eIF4G cleavage, and disrupts type I interferon signaling by degrading IFNAR1 and cleaving MAVS and MDA5, making it indispensable for viral pathogenesis [4]. Unlike conventional inhibitors that block activity only transiently, PROTAC-580 should catalytically direct $2A^{pro}$ to CRBN-mediated ubiquitination and proteasomal degradation, enabling complete removal of

the target protein, potentially lowering resistance risk, and expanding the range of druggable viral proteins [5, 6].

Using integrative structural biology, including X-ray crystallography, molecular docking, and crosslinking mass spectrometry, we rationally designed PROTAC-580 to achieve high selectivity and sustained degradation of $2A^{pro}$. To support these efforts, we established an optimized recombinant expression system in E. coli, incorporating solubility-enhancing fusion tags, buffer screening, and refined purification workflows to obtain milligram-scale quantities of active, monodisperse protein for structural analysis and degradation assays.

Aligned with the PANVIPREP consortium's vision for broad-spectrum antiviral development, PROTAC-580 marks a paradigm shift from inhibition to targeted protein degradation, offering a promising therapeutic strategy not only against enteroviruses but also as a platform for combating other RNA.

L22

BEYOND ONCOGENES: HOW RAS–MAPK VARIANTS INFLUENCE NEURODEVELOPMENT

P. Havlickova, A. Koutska, I. Kuta Smatanova, M. Fenckova

Faculty of Science, University of South Bohemia in Ceske Budejovice, Branisovska 1760, Ceske Budejovice, 37005, Czech Republic

fenckm00@prf.jcu.cz

The Ras–MAPK pathway, best known for its role in oncogenesis, is also critical for brain development. Germline mutations in pathway components cause RASopathies—the most common monogenic cause of intellectual disability (ID) and autism spectrum disorder (ASD)—and large-scale sequencing studies continue to uncover numerous additional variants in individuals with neurodevelopmental disorders (NDDs). Most are missense substitutions with uncharacterized functional effects, yet they often cluster within structural "hotspots" that control nucleotide binding, GTP hydrolysis, dimerization, or autoinhibitory regulation [1-3].

Here, large-scale genomic datasets are combined with high-resolution structures of Ras, B-Raf, MEK, and ERK to map these variants and infer their mechanistic consequences. Structural patterns reveal recurrent modes of dysregulation and show parallels with oncogenic mutations, indicating potential opportunities for targeted drug repurposing.

This structural–functional perspective refines pathogenicity assessment, explains phenotypic variability, and identifies priorities for functional validation. By shifting from purely statistical classification to mechanism-based interpretation, it establishes a framework for developing mutation-specific therapeutic strategies in Ras–MAPK–related neurodevelopmental disease.

1. Rauen K. A. (2013). The RASopathies. Annual review of genomics and human genetics, 14, 355–369. https://doi.org/10.1146/annurev-genom-091212-153523
2. Geoffray, M. M., Falissard, B., Green, J., Kerr, B., Evans, D. G., Huson, S., Burkitt-Wright, E., & Garg, S. (2021). Autism Spectrum Disorder Symptom Profile Across the RASopathies. Frontiers in psychiatry, 11, 585700. https://doi.org/10.3389/fpsyt.2020.585700
3. Wang, T., Kim, C. N., Bakken, T. E., Gillentine, M. A., Henning, B., Mao, Y., Gilissen, C., SPARK Consortium, Nowakowski, T. J., & Eichler, E. E. (2022). Integrated gene analyses of de novo variants from 46,612 trios with autism and developmental disorders. Proceedings of the National Academy of Sciences of the United States of America, 119(46), e2203491119. https://doi.org/10.1073/pnas.2203491119.

This work is supported by by a grant from the Czech Science Foundation (rant no. 23-07810S) and an EMBO Installation grant (grant no. IG-5310-2023) to M. Fenckova.

Session VII, September 10, Wednesday

L23

HARD X-RAYS WITH ORBITAL MOMENTUM, PROPERTIES AND DYNAMICAL DIFFRACTION

Václav Holý[1], Juraj Krempaský[2], Ondřej Caha[3], Ján Minár[4]

[1]Faculty of Mathematics and Physics, Charles University, Prague
[2]Paul Scherrer Institute PSI, Switzerland
[3]Faculty of Science, Masaryk University, Brno
[4]University of West Bohemia, Pilsen, Czech Republic

Hard X-ray beams with non-zero angular momentum are generated by diffraction on a specially designed spiral-like zone plate. In the talk the simulations of the wavefield behind the zone plate will be presented based on a rigorous evaluation of the exact Huygens-Fresnel diffraction integral beyond the paraxial approximation. Unlike conventional vortex light in visible or IR range, vortex X-rays diffract in a crystal lattice showing peculiar diffraction effects demonstrated both theoretically and experimentally. Possible effect of an X-ray vortex beam on static poling of ferroelectric GeTe will be discussed.

L24

Study of local atomic structure of disordered materials with the aid of *in-situ* synchrotron experiments

ŠTÚDIUM LOKÁLNEJ ATOMÁRNEJ ŠTRUKTÚRY NEUSPORIADANÝCH MATERIÁLOV POMOCOU *IN-SITU* SYNCHROTRÓNOVÝCH EXPERIMENTOV

Jozef Bednarčík

Univerzita Pavla Jozefa Šafárika v Košiciach, Prírodovedecká fakulta

V tejto prednáške budú demonštrované možnosti vysokoenergetických fotónových zväzkov, produkovaných na zdroji synchrotrónového žiarenia 3. generácie PETRA III v DESY Hamburg, pri štúdiu štruktúrnych zmien vyvolaných tepelným spracovaním tesne pod teplotou kryštalizácie amorfnej zliatiny na báze Fe. Budú prezentované výsledky štruktúrnej relaxácie amorfnej zliatiny pri jej cyklickom tepelnom namáhaní. Získané výsledky budú analyzované pomocou dvoch prístupov: 1) v recipročnom priestore na základe pozorovania zmien tvaru prvého výrazného difúzneho maxima a následne 2) pomocou párovej distribučnej funkcie. Hlavný dôraz v príspevku bude kladený na uvedenie konceptu párovej distribučnej funkcie a jej využitia pri štúdiu silne neusporiadaných systémov.

L25

LIGHT-INDUCED PHASE SEGREGATION AND STRUCTURAL RELAXATION IN MIXED-HALIDE PEROVSKITES

M. Dopita, V. Holý, L. Horák and P. Machovec

Department of Condensed Matter Physics, Faculty of Mathematics and Physics, Charles University, Ke Karlovu 5, 121 16 Prague 2, Czech Republic
milan.dopita@matfyz.cuni.cz

Mixed-halide perovskites are promising for high-efficiency multi-junction solar cells but are prone to light-induced halide segregation (Hoke effect), which alters their absorption spectrum and degrades optoelectronic performance. In this study we combined in operando and in situ X-ray scattering methods with complementary optical and electrical measurements to track structural changes, strain evolution, and domain morphology during illumination. Kinetic modelling using the Cahn–Hilliard formalism linked halide migration to observed diffraction peak broadening, indicating formation of Br-rich and Br-poor domains. Even after prolonged relaxation, residual strain and lattice parameter heterogeneity persist, underscoring the complex interplay between illumination, composition, and structural stability in these materials. Our results highlight the complex interplay between illumination, compositional changes, residual strain, and other factors such as humidity, single-crystal quality, or thin-film properties, emphasizing the need to fully understand all influences on the phase segregation effect and to mitigate them for the production of operationally stable devices.

CL1

ANTON PAAR, SAXSPOINT 500/700 - NEW EQIPMENT FRO SMALL-ANGLE SCATTERING

Jiří Špringer

Anton Paar

Anton Paar introduces SAXSpoint 500 and SAXSpoint 700, state-of-the-art laboratory beamlines offering unparalleled capabilities in SAXS/WAXS/GISAXS/USAXS/RheoSAXS analysis. Engineered for versatility, the SAXSpoint 500 is optimized for high-throughput and routine measurements, offering robust performance for quality control and standard research tasks. The SAXSpoint 700 extends capabilities with an ultra-low background design, enabling the characterization of weakly scattering and highly dilute samples at the highest scientific standards. SAXSpoint 700 features a spacious and innovative measurement chamber, allowing users to conduct experiments under ambient, non-ambient, and air conditions. The RheoSAXS integration in SAXSpoint 700 allows users to study structural and rheological properties simultaneously, combining the capabilities of SAXS with DSR 502 rheometer.

CL2

ENABLING NANOSCALE INSIGHT: ADVANCED X-RAY SCATTERING SOLUTIONS FROM XENOCS

Szymon Stolarek

Xenocs SAS, 1-3 Allée du Nanometre 38000 Grenoble France

Understanding structure at the nanoscale is critical to innovation across fields ranging from biotechnology to materials science. Founded with the mission to make advanced characterization tools accessible to researchers worldwide, Xenocs develops state-of-the-art laboratory solutions based on small- and wide-angle X-ray scattering (SAXS/WAXS) and X-ray imaging, enabling high-quality, multiscale structural analysis for both research and industrial applications.

This presentation will introduce two of Xenocs' flagship solutions: the Xeuss Pro and the Nano-inXider. Designed for maximum versatility, the Xeuss Pro is a modular SAXS/WAXS/GISAXS/USAXS/Imaging platform offering synchrotron-grade performance in the laboratory. It supports a range of X-ray sources—including microfocus

sources with various target materials, MetalJet, and rotating anode (RAG) options—as well as a focused AuX source for small-spot or high-resolution applications. With integrated USAXS and motorized SWAXS it enables fully automated and continuous measurements from atomic to micron scales. In addition, the InXight X-ray imaging module with dark-field and phase-contrast option further extends capabilities by revealing orientation, heterogeneity, and interfaces in complex materials. All these capabilities are seamlessly managed through the Xenocs Xplore control software, which provides an ergonomic interface for experiment planning, scriptable control (e.g. Python), and real-time equipment monitoring to track system performance remotely.

The Nano-inXider, by contrast, offers a compact, easy-to-use SAXS/WAXS system for routine nanostructural analysis. It combines a small footprint and intuitive operation with high-quality, reproducible data — making it ideally suited for quality control, process monitoring, and material development in both academic and industrial laboratories.

To complement these instruments, Xenocs provides XSACT Pro, an all-in-one SAXS/WAXS data analysis platform. It supports a wide range of analytical workflows including two advanced modules: one for AI-assisted shape classification and another for automated model fitting, helping researchers extract structural insights from complex scattering patterns quickly and reliably.

Figure 1. Xeuss Pro horizontal platform for SAXS/WAXS/GISAXS/USAXS and imaging alongside the Nano-inXider compact vertical system.

Trusted by leading academic institutions and companies across diverse sectors, Xenocs instruments accelerate material development and process optimization. Through high-performance, scalable, and user-focused solutions, Xenocs advances its mission: enabling nanoscale insight through continuous innovation.

Session VIII, September 10, Wednesday

L26

XRDLICIOUS: AN ONLINE TOOL FOR POWDER DIFFRACTION PATTERNS AND (P)RDF SIMULATIONS

M. Lebeda[1,2,3], J. Drahokoupil[1,3], P. Veřtát[1], P. Vlčák[3]

[1]Institute of Physics of the Czech Academy of Sciences, Na Slovance 2, 18200 Prague 8, Czech Republic
[2]Faculty of Nuclear Sciences and Physical Engineering, Czech Technical University in Prague, Trojanova 339/13, 12000 Prague 2, Czech Republic
[3]Faculty of Mechanical Engineering, Czech Technical University in Prague, Technická 4, 16607 Prague 6, Czech Republic
lebedmi2@cvut.cz

XRDlicious [1] is an online browser-based platform for computing powder X-ray diffraction (XRD) and neutron diffraction (ND) patterns, as well as partial and total radial distribution functions ((P)RDF), directly from crystal structure files. It supports common formats (CIF, POSCAR, XYZ, LMP) and can import data via file upload or integrated search in the Crystallography Open Database (COD), Materials Project (MP), and AFLOW. Multiple structures can be uploaded simultaneously, enabling direct comparison of computed diffractograms. Structures can be edited within the interface and exported in various formats. The tool also converts experimental diffraction data between wavelengths, d-space/q-space, fixed or automatic divergence slits, and supports conversion between XRDML (PANalytical) and RAS (Rigaku) formats into standard XY files and vice versa. Requiring no installation, XRDlicious runs on any device (computers, tablets, mobile phones) and across operating systems. Its intuitive interface and ease of use makes it promising for both research and teaching. The platform is freely available at xrdlicious.com, hosted on Streamlit community free cloud server, with source code and instructions for optional local installation at github.com/bracerino/xrdlicious.

1. (PREPRINT) Lebeda, M. et al. (2025). *Journal of Applied Crystallography 58*, https://doi.org/10.1107/S1600576725005370.

continues on next page

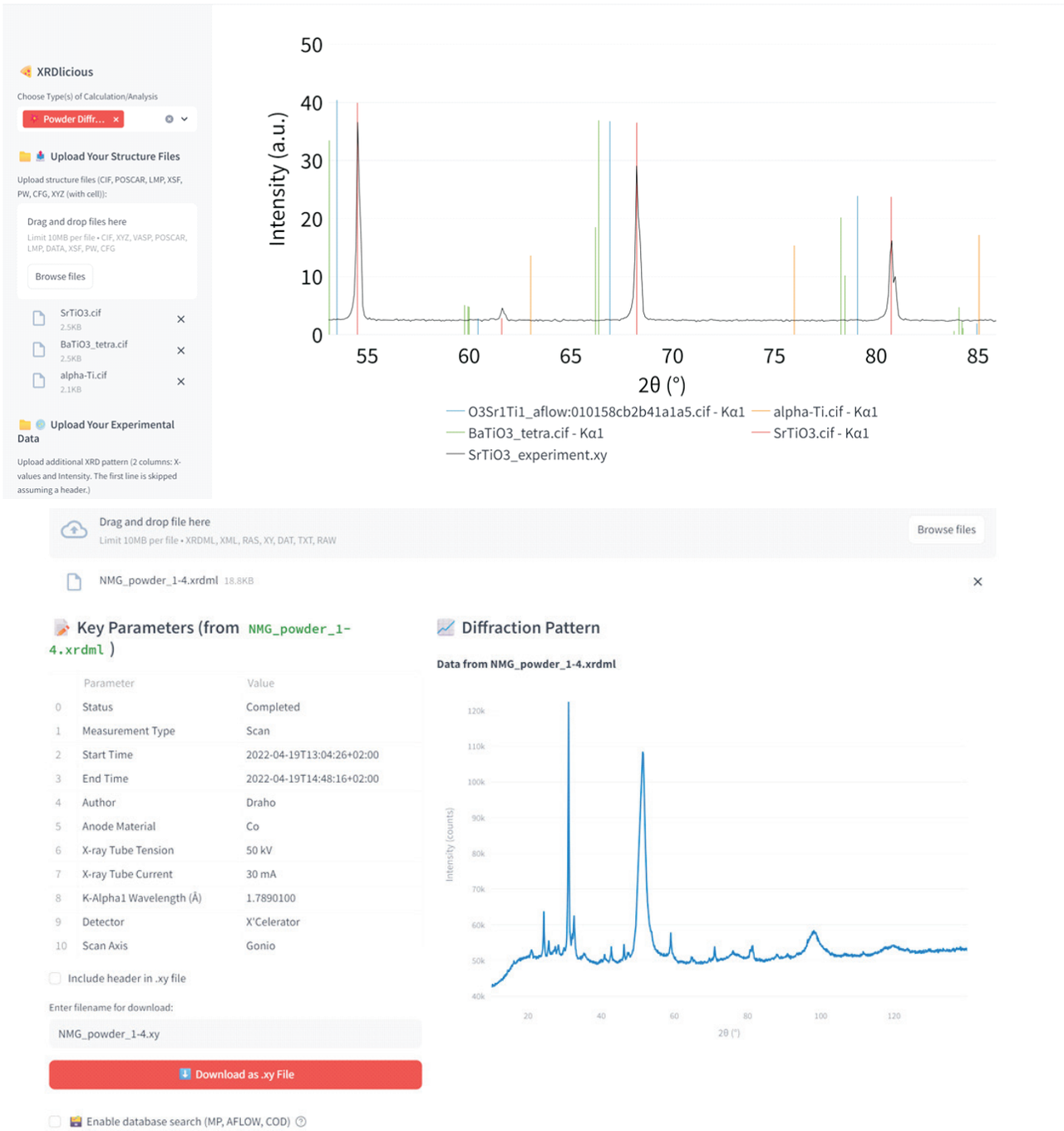

Figure 1. Example of XRDlicious output: calculated XRD patterns for multiple structures compared with experimental data, and demonstration of XRDML to XY file conversion.

.

L27

BASIC CRYSTALLOGRAPHIC ALGORITHMS IN THE ML LANGUAGE

Z. Matěj

MAX IV Laboratory, Lund University, Lund, Sweden
zdenek.matej@maxiv.lu.se

Machine learning (ML) is increasingly finding applications in crystallography and materials science, enabling data-driven discovery of structural patterns, accelerating phase identification, and predicting material properties from complex diffraction and imaging datasets. In addition to these novel applications, traditional algorithms - used in crystallography for decades - are now being reimplemented using ML-based methods or simply executed within high-performance ML frameworks to benefit from their computing capabilities.

Among the next generation of scientists it is common a crystallography problem - that would be traditionally resolved by progressive analysis, followed by application of tailored numerical methods - is tackled by data-driven ML approach. While generic, unoptimized ML solutions often require more computational resources than traditional methods, the availability of optimized ML hardware and advanced software frameworks, built on robust mathematical libraries and developed by both the research community and industrial partners, can offer efficient alternatives.

This contribution aims to provide a gentle introduction to implementing several computational algorithms commonly used in the analysis of diffraction data in materials science and crystallography. The selected examples focus on well-understood, foundational algorithms that will be reformulated as neural networks. The process of solving these problems using data-driven approaches will be illustrated, including the full workflow and a discussion of its limitations, strengths, and potential ML-based extensions. Demonstrations will include peak parameter refinement using the least squares method, electron density map calculation, and a basic iterative algorithm for phase problem solving.

L28

MACE-INTERACTIVE: A BROWSER-BASED GUI FOR ATOMISTIC SIMULATIONS WITH MACE FOUNDATION MODELS

J. Drahokoupil[1,3], M. Lebeda[1,2,3]

[1]*Institute of Physics of the Czech Academy of Sciences, Na Slovance 2, 18200 Prague 8, Czech Republic*
[2]*Faculty of Nuclear Sciences and Physical Engineering, Czech Technical University in Prague, Trojanova 339/13, 12000 Prague 2, Czech Republic*
[3]*Faculty of Mechanical Engineering, Czech Technical University in Prague, Technická 4, 16607 Prague 6, Czech Republic*
lebedmi2@cvut.cz

Pre-trained foundation models in machine-learning interatomic potentials (MLIPs) allow researchers to perform accurate and efficient atomistic simulations without the need to search for or fit a potential for each studied system. These universal models approach the accuracy of density functional theory (DFT) while being orders of magnitude faster, making it feasible to study systems with even more than thousands of atoms, well beyond the practical size limits of DFT.

We have developed MACE-Interactive, a browser-based graphical interface designed to streamline calculations with the MACE MLIP foundation models [1]. The application supports multiple simultaneous structure uploads (POSCAR, CIF, LMP, XYZ with lattice), and presents calculated results in an easily readable way, allowing direct comparison between structures. Currently, the MACE-Interactive provides single-point energies, geometry optimizations, elastic properties, and phonon calculations, as well as genetic algorithm for identifying the energetically most favourable arrangements of substitutions or vacancies. The tool can also generate fully configured Python scripts based on the parameters set by the user in the interface for external console execution. The source code and installation instructions are provided at github.com/bracerino/mace-md-gui, with a video tutorial illustrating the application use and capabilities at: https://youtu.be/xh98fQqKXaI.

1. BATATIA, Ilyes, et al. A foundation model for atomistic materials chemistry. *arXiv preprint arXiv:2401.00096*, 2023.

continues on next page

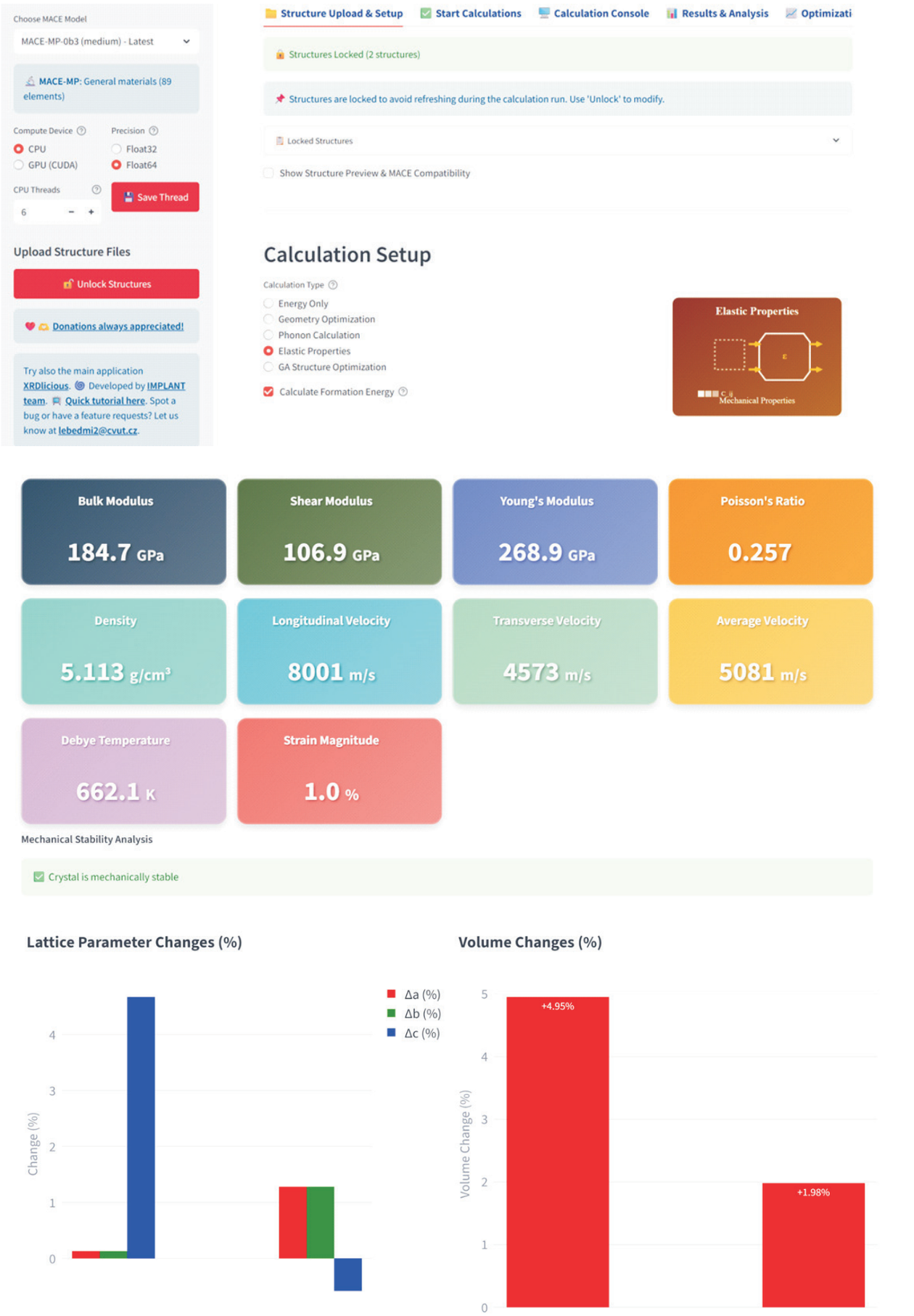

Figure 1. Example of MACE-Interactive: Calculation setup, computed elastic properties, and differences in lattice parameters before and after geometry optimization.

Session IX - Large European Neutron Facilities, September 11, Thursday

L29

INSTITUTE LAUE-LANGEVIN - INSTRUMENT AND INFRASTRUCTURE UPGRADES, THE SCIENCE STRATEGY AND NEW RESEARCH OPPORTUNITIES

M. Johnson

Institut Laue Langevin, Grenoble, France
johnson@ill.eu

The comprehensive Endurance upgrade programme was completed in 2024. With a budget of 50+ M€, about 30 projects have been delivered, including neutron guide systems, new and upgraded instruments, sample environment and data and software services. More intense neutron beams combined with more efficient detector systems provide major new capability for measuring ever smaller samples, including in extreme sample environments, and weaker signals. In addition, significantly shorter measuring times facilitate parametric studies and increase throughput and, therefore, overall capacity. Thus the upgrade programme as a whole, supported by ongoing and new projects, ensures that research capability at the ILL will continue to be world leading for the next decade, offering new opportunities for cutting-edge science. In this context, the ILL has elaborated a science strategy to optimise the use of its state-of-the-art scientific infrastructure over the next decade and enhance the delivery of societal impact with neutrons.

The Endurance programme, ongoing and new projects, and the science strategy will be presented, including recent science highlights, and set in the context of future reactor operation, given the recent, excellent decision that ILL will now operate at least until the end of 2033.

L30

DIFFRACTION AT MLZ

M. Hofmann

Heinz Maier-Leibnitz Zentrum (MLZ), Technical University of Munich (TUM), Garching, Germany

The Heinz Maier-Leibnitz Zentrum or in short, the MLZ, is a cooperation between the Technical University of Munich (TUM), the Jülich Centre for Neutron Scatterring (JCNS) and the Helmholtz-Zentrum hereon. This cooperation is the scientific umbrella for the exploitation of Germany's sole neutron source FRM II in Garching close to Munich. As such it is responsible for the installation and operation of all the positron and neutron scattering instruments installed at FRM II [1].

Besides a brief introduction of the facility at large, this presentation will focus primarily on the diffraction suite of instruments of MLZ. In particular I will highlight recent developments and upgrades in the existing instrumentation as well as new diffractometers, which will be part of the user program once the FRM II restarts after a longer shutdown period in early 2026. In addition, I will also show some scientific highlights from experiments in energy materials, the life sciences as as well as alloy development, of which many were also done in close cooperation with scientific groups from the Czech Republic.

1. https://mlz-garching.de/englisch/about-mlz.html .

L31

ESS NEWS AND FIRST SCIENCE OPPORTUNITIES

Přemysl Beran[1,2]

[1]*Czech Academy of Sciences, Nuclear Physics Institute, Hlavni 130, Rez, 25068, Czech Republic*
[2]*European Spallation Source, ERIC, PO Box 176, Lund, 22100, Sweden*
premysl.beran@ess.eu

The European Spallation Source (ESS) [1], located in Lund, Sweden, is nearing completion and represents a significant advancement in neutron science research. Designed to be the world's most powerful neutron source, the ESS has achieved several significant milestones in its construction. The high-energy proton linac, responsible for driving the spallation process, has been successfully tested, and critical components such as the neutron target station and instrument infrastructure are now close to hot commissioning. The facility's technical complexity and scale, incorporating cutting-edge technologies in accelerator physics, neutron optics, and detection systems, reflect its ambition to transform the way neutrons are harnessed for scientific exploration. As construction progresses, ESS has transitioned into a new operational phase, focusing on the commissioning of its first suite of instruments and preparing them for experimental research and the users. An update on the status and the near prospects will be presented.

The "first science" opportunities at the ESS will validate the performance of the initial instruments, including LOKI, ODIN, DREAM, and others, marking the beginning of scientific operations and the user program. Each of these instruments is tailored to address specific scientific challenges. For instance, LOKI, a small-angle neutron scattering instrument, will provide insights into nanoscale structures and dynamics, enabling research into soft matter, polymers, and biological systems. ODIN is designed to perform high-resolution neutron imaging, making it ideal for investigating structural properties in engineering materials and complex natural systems. DREAM leverages neutron diffraction techniques to study atomic arrangements and phase transitions in materials critical to energy and quantum technologies. By conducting the first experiments, the ESS will establish baseline operations for its instruments and demonstrate the unprecedented capacity of its neutron beamlines. Here, it is equally important to underline the contributions of early users and the broader user communities, whose expertise, feedback, and collaborative research will be vital to refining the ESS's capabilities and ensuring its impact on scientific advancement across various fields. The way to get involved will be depicted.

1. K.H. Andersen, et al., The instrument suite of the European Spallation Source, Nuclear Instruments and Methods in Physics Research Section A: Accelerators, Spectrometers, Detectors and Associated Equipment, **957**, (2020) 163402.

Session X - Neutron Science in Czech Republic I, September 11, Thursday

L32

NEUTRON DIFFRACTION LABORATORY IN ŘEŽ AND ITS USER PROGRAM

G. Farkas, V. Ryukhtin, P. Milkula, Ch. Hervoches, O. Levytska, P. Strunz and J. Šaroun

Nuclear Physics Institute, v.v.i., Czech Academy of Sciences, Husinec–Řež, čp. 130, 250 68 Řež
saroun@ujf.cas.cz

The neutron diffraction laboratory in Řež is part of the Centre of Accelerators and Nuclear Analytical Methods (CANAM) – a large research infrastructure hosted by the Nuclear Physics Institute of the CAS. It is one of the few European facilities providing the scientific community with neutron scattering methods and thus helping to fill the current gap in the availability of neutron beams. The laboratory equipment consists of five neutron diffractometers in the thermal neutron channels of the 10 MW research reactor LVR-15 (operated by Research Centre Řež, Ltd.), four of which are used for experiments mainly in the field of materials research and offered to external users within an open access programme. The TKSN-400 instrument is dedicated to in situ thermomechanical loading experiments for studying deformation mechanisms in metallic materials. For this purpose, it has been equipped with a 20 kN uniaxial stress rig designed in-house, with current heating, as well as a small stress rig in an Eulerian cradle for analysing the evolution of lattice strain components in highly textured materials. Another instrument, TKSN-100, is used for non-destructive mapping of residual stresses in bulky samples, with precise positioning enabled by a robotic arm. The powder diffractometer MEREDIT helps to solve various problems of structure analysis were neutrons provide valuable complementary information, in particular on evolution of magnetic ordering or site occupation by atoms of similar proton numbers. Phase transformations can be observed in situ within a wide thermal range of about 10 to 1300 K using a closed-cycle He cryostat or vacuum furnace. This suite of instruments is complemented by the high-resolution small-angle scattering diffractometer MAUD, which is particularly well suited to studying microstructural features such as porosity or precipitation within the size range of approximately 50–2000 nm. Although there is no dedicated instrument available for neutron imaging, it is possible to perform neutron tomography with a monochromatic beam at the MEREDIT instrument, with a field of view of up to 4x4 cm¸ and a resolution of < 0.2 mm.

In recent years, the facility has offered around 300 instrument days per year as part of its open access programme, most of which have been allocated to experiments proposed by external users. Applications for experiments are welcome at any time, provided they are feasible and scientifically relevant. These are evaluated by a selection panel comprising internal and external experts.

L33

CZECH NEUTRON ASSOCIATION - ESTABLISHMENT, MISSION, AND OBJECTIVES

Milan Klicpera[1], Jan Šaroun[2], Petr Čermák[1], Pavel Strunz[2], Dominika Zákutná[3]

[1]*Faculty of Mathematics and Physics, Charles University, Prague*
[2]*Institute of Nuclear Physics, Czech Academy of Sciences, Řež*
[3]*Faculty of Mathematics and Physics, Charles University, Prague*

We are reaching out to inform you about the establishment of a new professional association - the **Czech Neutron Association (Česká neutronová asociace, z. s.)**, founded to unite, support, and represent the community of Czech users of neutron radiation.

The Association's mission is to:

- Bring together researchers and institutions using neutron radiation across disciplines.
- Promote the potential and results of research based on neutron methods.
- Facilitate dialogue between the scientific community, the public, and government authorities.
- Represent the interests of the Czech neutron community in European and other international institutions and structures with relevant thematic focus.

We believe that the Czech Neutron Association will significantly contribute to the coordination of national neutron infrastructure, strengthen international cooperation, and facilitate access for Czech researchers to world-class experimental facilities and expertise.

Membership in the Association offers the opportunity to participate in the development of neutron research in the Czech Republic, engage in joint scientific initiatives, and become part of a representative platform for neutron-based science at both national and international levels. More information about the Association's activities, its statutes, and the membership application will be presented during Struktura 2025; and can be found at neutrons.cz.

Committee of the Czech Neutron Association.

L34

RESIDUAL-STRESS DISTRIBUTION IN COMPONENTS FABRICATED WITH INVOLVEMENT OF ADDITIVE MANUFACTURING

Pavel Strunz[1,*], Josef Izák[2], Štěpán Jedlan[3], Olena Levytska[1], Josef Hodek[4], Gergely Németh[1,5], Jan Šaroun[1], Radim Kocich[2,6], Marek Pagáč[7] and Kostyantyn Tuharin[1,8]

[1]Nuclear Physics Institute of the Czech Academy of Sciences, Husinec—Řež 130, 250 68 Řež, Czech Republic; levytska@ujf.cas.cz (O.L.); nemeth@ujf.cas.cz (G.N.); saroun@ujf.cas.cz (J.Š.); tuharin@ujf.cas.cz (K.T.)

[2]Faculty of Mechanical Engineering, Brno University of Technology, Technická 2896, 616 00 Brno, Czech Republic; 183119@vutbr.cz

[3]Faculty of Nuclear Sciences and Physical Engineering, Czech Technical University in Prague, Prague, Czech Republic

[4]COMTES FHT a.s., Dobřany, Czech Republic

[5]Paul Scherrer Institute—PSI, 5232 Villigen, Switzerland

[6]Faculty of Materials Science and Technology, VŠB-Technical University of Ostrava, 17. Listopadu 2172/15, 708 00 Ostrava, Czech Republic; radim.kocich@vsb.cz

[7]Faculty of Mechanical Engineering, VŠB-Technical University of Ostrava, 17. Listopadu 2172/15, 708 00 Ostrava, Czech Republic; marek.pagac@vsb.cz

[8]Faculty of Mathematics and Physics, Charles University, Ke Karlovu 2027/3, 121 16 Prague, Czech Republic

**strunz@ujf.cas.cz*

Additive manufacturing opened new possibilities in fabrication of components. However, at the same time, it introduced new tasks for metalurgists and materials engineers as the microstructure of the components prepared by additive manuffacturing is significantly different than the microstructure of the conventionally fabricated components. One of the characteristics largely influenced by additive manufacturing is the residual stress distribution. Residual stresses play a crucial role in determining the performance and lifetime of engineered components.

Some examples taken from the field of materials fabricated by additive manufacturing are shown. Residual stresses were measured using neutron diffraction in these demonstrations. The use of neutron diffraction is indispensable for the measurement of residual stresses in the bulk of the material. It is a non-destructive method; therefore, the sample can be later used for other examinations.

The impact of manufacturing strategies on the development of residual stresses in Dievar steel is presented. Two fabrication methods were investigated: conventional ingot casting and selective laser melting (SLM) as an additive manufacturing process. Subsequently, plastic deformation in the form of hot rotary swaging at 900°C was applied. Microstructural and phase analysis, precipitate characterization, and hardness measurement—carried out to complement the investigation by neutron diffraction—showed the microstructure improvement by rotary swaging. The study reveals that the manufacturing method has a significant effect on the distribution of residual stresses in the bars. The results showed that conventional ingot casting resulted in low levels of residual stresses (up to ±200 MPa), with an increase in hardness after rotary swaging from 172 HV1 to 613 HV1. The SLM-manufactured bars developed tensile hoop and axial residual stresses in the vicinity of the surface and large compressive axial stresses (-600 MPa) in the core due to rapid cooling. The subsequent thermo-mechanical treatment via rotary swaging effectively reduced both the surface tensile (to approximately +200 MPa) and the core compressive residual stresses (to -300 MPa). Moreover, it resulted in a predominantly hydrostatic stress character and a reduction in von Mises stresses, offering relatively favorable residual stress characteristics and, therefore, a reduction in the risk of material failure. In addition to the significantly improved stress profile, rotary swaging contributed to a fine grain (3–5 μm instead of 10–15 μm for the conventional sample) and increased the hardness of the SLM samples from 560 HV1 to 606 HV1. These insights confirm the utility of rotary swaging as a post-processing technique that not only reduces residual stresses but also improves the microstructural and mechanical properties of additively manufactured components.

Residual stresses were also measured in samples manufactured by two different AM technologies within one component: the bottom half prepared using either Laser Powder Bed Fusion (L-PBF) or Direct Energy Deposition (L-DED), and the second half of the component vice versa, i.e. using L-DED or L-PBF, respectivelly. A combination of fabrication by different additive technologies is not a commonly used procedure in practice. Cubic regions (25mm × 25mm × 25mm) of 316L steel were printed either by L-PBF or by L-DED on the steel substrate and afterwards finished to a height of 50 mm by the second technology. The aim was to determine the residual stresses that each technology introduces into the samples and a comparison with FEM prediction: the stresses measured by neutron diffraction are to be used for validation of the FEM model, which will be applieded as an optimization tool in the combination of AM production methods.

L35

VALIDATION OF CONTOUR CUT MODEL FOR RESIDUAL STRESSES IN AM-REPAIRED SIMULATED DEFECT BY NEUTRON DIFFRACTION

Josef Hodek, Štěpán Jedlan, Martin Ševeček, Jan Šaroun, Olena Levytska, Michal Brázda, Antonín Prantl, Pavel Strunz

Institute of Physics, Czech Academy of Sciences, Řež

This study validates the accuracy and reliability of the Contour Cut Method (CCM) for residual stress assessment using neutron diffraction (ND) in a critical case — the repair of a simulated defect in a 316L component by Laser-Directed Energy Deposition (L-DED). CCM combines finite element modeling (FEM) with a series of precision cuts to recover residual stress data.

A strong agreement was observed between ND and CCM results. Neutron diffraction measurements along the sample's central line revealed local stress maxima and minima, with the highest tensile stresses located in the L-DED region and the central part of the substrate.

The demonstrated correlation supports the applicability of CCM as a reliable technique for residual stress evaluation in various industrial contexts.

L36

PUMP-PROBE NEUTRON INELASTIC SCATTERING EXPERIMENTS.

J. Kulda

Institute Laue-Langevin, CS 20156,38042 Grenoble Cedex 9, France
kulda@ill.fr

The neutron and, more recently, X-ray spectroscopy have been standard workhorses for investigations of condensed matter dynamics at atomic resolution. Nevertheless, the inherently weak interaction of both probes with matter, accompanied by the tiny flux densities of neutron beams and by the huge X-ray photon energy as compared to the energy scale of elementary excitations in condensed matter, have limited their implementation to simple scattering, leaving no options for analogies to optical experiments with coherently split beams.

Experiments using synchronized pulsed X-ray and laser beams to investigate the time evolution of non-equilibrium states of condensed matter, both in the structural and in the magnetic domains, are quickly becoming routine at XFEL (X-ray Free Electron Lasers) beams exhibiting picosecond time-structures, accompanied by extreme transversal coherence (e.g. [1]). With neutrons the progress is slower, but reports on successful attempts of time-resolved work have appeared recently as well [2,3] and, after all, a dedicated pump-probe setup has been developed and tested at the SNS Hyspec spectrometer at the ORNL [4].

In this presentation we shall recall the basic principles of scattering theory based on timedependent correlation functions and review the present state of neutron experimental techniques addressing transient processes in matter, their principal limitations and development opportunities.

1. Y. Lee, K. Y. Oang, D. Kim, and H. Ihee, "A comparative review of time-resolved x-ray and electron scattering to probe structural dynamics," *Structural Dynamics*, vol. **11**, no. 3. AIP Publishing, May 01, 2024. doi: 10.1063/4.0000249.
2. M. Wang et al., □"Optically Induced Static Magnetization in Metal Halide Perovskite for Spin□]Related Optoelectronics," *Advanced Science*, vol. **8**, no. 11. Wiley, May 02, 2021. ' doi: 10.1002/advs.202004488.
3. Y. Wang et al., □"Monopolar and dipolar relaxation in spin ice $Ho_2Ti_2O_7$," *Science Advances*, vol. **7**, no. 25. American Association for the Advancement of Science (AAAS), Jun. 18, 2021. doi: 10.1126/sciadv.abg0908.
4. C. Hua, D. A. Tennant, A. T. Savici, V. Sedov, G. Sala, and B. Winn, □"Implementation of a laser.neutron pump.probe capability for inelastic neutron scattering," *Review of Scientific Instruments,* vol. **95**, no. 3. AIP Publishing, Mar. 01, 2024. doi: 10.1063/5.0181310.

Session XI - Neutron Science in Czech Republic II, September 11, Thursday

L37

EXPERIMENTAL DETERMINATION OF CRITICAL RESOLVED SHEAR STRESSES BY NEUTRON DIFFRACTION

G. Farkas[1], A. Ludwik[2], M. Wroński[2], P. Kot[3], A. Baczmański[2]

[1]Nuclear Physics Institute ASCR v.v.i., Czech Academy of Sciences, Řež

[2]AGH University of Science and Technology, Faculty of Physics and Applied Computer Science, al. Mickiewicza 30, 30-059 Krakow, Poland

[3]NOMATEN Centre of Excellence, National Centre of Nuclear Research, A. Sołtana 7, 05-400 Otwock-Świerk, Poland

This study investigates the plastic deformation mechanisms of AZ31 magnesium alloy using *in-situ* neutron diffraction and Crystallite Group Method (CGM). *In-situ* neutron diffraction enables measurement of the stress tensor for specific grain families within a policrystal by determining lattice strains from diffraction peaks associated with the same grain family, observed from multiple orientations and hkl reflections. Tracking the evolution of the stress tensor makes it possible to experimentally determine the Critical Resolved Shear Stresses (CRSS) and to characterise the hardening behaviour of different slip and twinning systems.

Tensile tests were performed along the rolling direction (RD), while compression tests were conducted along the normal direction (ND), and at 30° (ND30) to the ND, allowing assessment of the anisotropic mechanical response. The CGM allowed direct determination of grain-level stresses for preferred crystallographic orientations, leading to unambiguous CRSS values and, notably, an improved estimate for the basal slip system from the ND30 test, compared to previous findings [1]. These experimentally derived CRSS values, along with the evolution of Resolved Shear Stresses (RSS), were used to validate and calibrate the Elastic-Plastic Self-Consistent (EPSC) model adapted for hexagonal crystal structures. The combined experimental-modelling approach enhances understanding of plastic anisotropy in AZ31 alloy and improves the predictive capability of the EPSC framework for magnesium alloys subjected to complex loading conditions.

1. Kot, P., Wroński, M., Baczmański, A., Ludwik, A., Wroński, S., Wierzbanowski, K., Scheffzük, C., Pilch, J., Farkas, G., 2023. A novel method of experimental determination of grain stresses and critical resolved shear stresses for slip and twin systems in a magnesium alloy. *Measurement* **221**, 113469.

L38

INVESTIGATIONS OF MAGNETIC VORTEX LATTICES AND SKYRMIONS USING NEUTRON SCATTERING

V. Ryukhtin

Nuclear Physics Institute ASCR v.v.i., Czech Academy of Sciences, Řež¨

Neutron scattering can be very efficiently used for studying of magnetic vortex lattices (VL) (or flux-line lattices (FLL)) in unconventional superconductors. Actually, very first experimental evidence of VL existence after their theoretical prediction by Abrikosov [1] was conducted by means of neutron scattering [2] in Nb. Exploring of small angle neutron scattering (SANS) for direct observation of FLL [3] got “second - breath” with discovering of high-Tc superconductors (HTSC), which are all of type-II and with higher upper critical field H_{c2}. SANS is exceptional tool for establishing the values of HTSC.

Sr_2RuO_4, an isostructural of the high-Tc material $La_{2-x}Sr_xCuO_4$, is the first 2D perovskite oxide that exhibits superconductivity without copper [3]. Unlike $La_{2-x}Sr_xCuO_4$, however, it exhibits Fermi liquid behavior in its normal state. Sr_2RuO_4 then became an attractive material to probe the mechanism of high-Tc superconductivity, and also to study p-wave superconductivity since it has a simple band structure compared to Uranium based systems, another p-wave superconducting family. To this date, however, some groups still claim that there is no credible evidence of p-wave superconductivity of Sr_2RuO_4. Here, some first results of FLL in Sr_2RuO_4 measurements conducted at KWS-3 SANS facility are reported.

The measurements of dynamics of skyrmion lattice using neutron spin-echo technique is reported as well. Skyrmions are vortex-like magnetics structures, created in helimagnet (here was used single crystal MnSi). According to recent theoretical studies the lowest-energy excitations of the system are the so-called ‘phason’ modes of the skyrmion lattice. Their dispersion curves for the propagation vector ($\mathbf{q}_z$) parallel to the magnetic field are expected

to be asymmetric along the strings of the skyrmions, indicating that the magnetic excitations have different q dependencies along $+\mathbf{q}_z$ and $-\mathbf{q}_z$. This prediction was tested by a Spin-Echo technique that is sensitive to these low-energy excitations and to their momentum and it was showed that an asymmetric magnetic dispersion is present in the skyrmion state [4].

1. A. A. Abrikosov, Zh. Eksp. Teor. Fiz. (1957) **32** 1442.
2. D. Cribier, *et al.* in Progress in Low Temperature Physics, (1967), **5** 161.
3. T. M. Riseman, *et al.* Nature (London) 396, 242 (1998).
4. Soda, M., *et al.* Asymmetric slow dynamics of the skyrmion lattice in MnSi. Nat. Phys. 19, 1476–1481 (2023).

L39

NOVEL PYROCHLORE-LIKE STRUCTURE IN RARE-EARTH IRIDATE SINGLE CRYSTALS

F. Hájek[1], D. Staško[1], K. Vlášková[1], J. Kaštil[2], M. Henriques[2], M. Klicpera[1]

[1]Charles University, Faculty of Mathematics and Physics, Department of Condensed Matter Physics, Ke Karlovu 5, 121 16 Prague 2, Czech Republic

[2]Institute of Physics of the Czech Academy of Sciences, Na Slovance 2, 182 21 Prague 8, Czech Republic

filip.hajek@matfyz.cuni.cz

The rare-earth $A_2Ir_2O_7$ pyrochlore iridates (A = Y, Pr-Lu) constitute a family of materials revealing a plethora of novel and exotic properties. The geometrically frustrated pyrochlore lattice hosts Ir^{4+} ions displaying strong spin-orbit coupling comparable to electron correlations. In combination with crystal field effects and important *f-d* exchange between the rare-earth and iridium sites, various magnetic and topological phases emerge. Among others, the topological phases include the topological Mott insulator [1], axion insulator [2] or Weyl semimetal [2,3] and the magnetic phases include the fragmented spin ice state with monopole-like excitations [4] and spin liquid states [5, 6].

The following work is focussed on the magnetic and structural properties of the A = Nd single crystal analogue. In contrast to previous works, e.g. [7], where $Nd_2Ir_2O_7$ adopts the pyrochlore structure, the present single crystals display a different, unusual crystal structure, attributed to a new Pb-based synthesis method. Magnetic properties, including two magnetic transitions at 41 K and 8 K, demonstrate notable similarities for the two crystal structures. The non-pyrochlore structure found using X-ray diffraction is analysed and compared to the pyrochlore structure, with a focus on the Ir pyrochlore-type tetrahedral sublattice with octahedral O^{2-} crystal fields found in both crystal lattices. The full crystal structure contains two Ir sublattices, three Nd sublattices and one Pb sublattice with a high degree of disorder in the form of vacancies. The magnetic structure, fundamentally tied to the tetrahedral lattice in the pyrochlore case, is examined in the non-pyrochlore samples employing neutron diffraction.

1. Y. Otsuka, T. Yoshida, K. Kudo, S. Yunoki, Y. Hatsugai, *Sci. Rep.*, **11**, (2021), 20270.
2. X. Wan, A. M. Turner, A. Vishwanath, S. Y. Savrasov, *Phys. Rev. B*, **83**, (2011), 205101.
3. X. Liu, S. Fang, Y. Fu, W. Ge, M. Kareev, J.-W. Kim, Y. Choi, E. Karapetrova, Q. Zhang, L. Gu, E.-S. Choi, F. Wen, J. H.Wilson, G. Fabbris, P. J. Ryan, J. W. Freeland, D. Haskel, W. Wu, J. H. Pixley, J. Chakhalian, *Phys. Rev. Lett.*, **127**, (2021), 277204.
4. E. Lefrançois, V. Cathelin, E. Lhotel, J. Robert, P. Lejay, C. V. Colin, B. Canals, F. Damay, J. Ollivier, B. FÍk, L. C. Chapon, R. Ballou, V. Simonet, *Nat. Commun.*, **8**, (2017), 209.
5. M. Kavai, J. Friedman, K. Sherman, M. Gong, I. Giannakis, S. Hajinazar, H. Hu, S. E. Grefe, J. Leshen, Q. Yang, S. Nakatsuji, A. N. Kolmogorov, Q. Si, M. Lawler, P. Aynajian, *Nat. Commun.* **12**, (2021), 1377.
6. Y. Machida, S. Nakatsuji, S. Onoda, T. Tayama, T. Sakakibara, *Nature* **463**, (2010), 210.
7. H. Takatsu, K. Watanabe, K. Goto, H. Kadowaki, *Phys. Rev. B* **90**, (2014), 235110.

L40

MAGNETIC STRUCTURE AND EXCITATIONS IN THE ANTIFERROMAGNET $Na_2BaMn(PO_4)_2$

David Svitak[1], Nikolaos Biniskos[1], Michal Stekiel[2], Bruce Normand[3], Karin Schmalzl[4], Andreas M. Läuchli[3], Flaviano Jose dos Santos[3], Petr Cermak[1]

[1]Charles University, Faculty of Mathematics and Physics, Department of Condensed Matter Physics
[2]Jülich Centre for Neutron Science (JCNS) at Heinz Maier-Leibnitz Zentrum (MLZ)
[3]PSI Center for Scientific Computing, Theory, and Data
[4]Jülich Centre for Neutron Science (JCNS) at Institut Laue Langeving (ILL).

The investigation of geometrically frustrated systems with antiferromagnetically (AFM) ordered spins attracts attention due to their potential to stabilize exotic quantum states, such as a spin liquid state, which holds promise for applications in quantum computing. Here we present our study of the triangular AFM compound $Na_2BaMn(PO_4)_2$ [1,2], which has an unusually high spin S = 5/2. In contrast, the isostructural compound with Co (S = 1/2) [3] has been studied extensively, as lower spin systems are typically more favorable for the formation of quantum spin liquids. We use single crystal neutron diffraction and inelastic neutron scattering to determine the magnetic structures and spin excitations for magnetic fields applied in the basal plane and along the *c*-axis of the trigonal symmetry. At zero magnetic field, the system undergoes two magnetic transitions at around 1.25 K (AFM2) and 1.1 K (AFM1). The out-of-plane incommensurate component k of the magnetic propagation vector (1/3, 1/3, k) changes significantly in these two AFM phases, which suggests non- negligible interlayer couplings.

Depending on the direction of the magnetic field, $Na_2BaMn(PO_4)_2$ shows several field-induced transitions. These transitions cause changes in the magnetic propagation vector before the system reaches the spin-polarized state. By combining neutron diffraction, low-temperature specific heat, and dc magnetization, we establish temperature–magnetic field phase diagrams for both field directions. Using ab-initio calculations and Monte Carlo simulations, we determine the exchange interactions, anisotropy parameters, and the phase diagrams. Our combined experimental and theoretical study shows that $Na_2BaMn(PO_4)_2$ is mainly a 2D system, with very weak 3D coupling that only acts as a "witness"to what happens in two dimensions. The separation between the two zero-field transitions (AFM1 and AFM2) depends on the XXZ nature of the anisotropy and the 3D coupling. The gap in the dispersion of the fully polarized phase is influenced by the XXZ anisotropy, single-ion anisotropies, and the magnetic field. Finally, we compare our results with the Co (S = 1/2) and Ni (S = 1) [4] counterparts and discuss their similarities and differences.

1. J. Kim, et. al., Journal of Physics: Condensed Matter, 34, p. 475803 (2022).
2. C. Zhang, et. al., Phys. Rev. B, 110, p. 214405 (2024).
3. N. Li, Q. Huang, et. al. Nature Communications, 11, p. 4216 (2020).
4. N. Li, Q. Huang, et. al. Phys. Rev. B, 104, p. 104403 (2021).

L41

INFLUENCE OF METAL OXIDE DEPOSITION ON MAGNETIC DISTRIBUTION AND COMPOSITION OF SUPRAPARTICLES

R. Conan[1,2], V. Müller[2], S. Müssig[2], K. Mandel[2], D. Zakutna[3]

[1]Department of Inorganic Chemistry, Charles University, Prague, Czechia
[2]Department of Chemistry and Pharmacy, Friedrich-Alexander University Erlangen Nürnberg (FAU), Erlangen, Germany
romain.conan@natur.cuni.cz

The development of multifunctional materials, which integrate multiple functional components, is a rapidly evolving field with significant implications across various technologies [1-2]. Colloidal nanocrystals are exceptional building blocks for constructing complex architectures in random or controlled assemblies [3-4]. By co-assembling different types of nanocrystals into larger colloidal particles, particularly at the mesoscale, novel supraparticles can be engineered. These supraparticles, typically micrometers in size and composed of functionalized nanoparticles and molecular building blocks [5], combine the properties of their constituent nanocrystals while maintaining their colloidal stability [6]. Recent interest in these materials stems from their versatility and broad applicability. For example, incorporating magnetic nanoparticles into supraparticles offers diverse applications, including magnetic separation, hyperthermia, drug delivery, and magnetic imaging. Furthermore, the inclusion of non-magnetic functional metal oxide ligands (e.g. Al_2O_3 for catalysis, ZnO for semicon-

ductors, TiO_2 for photocatalysis) can further epand the potential of these innovative supraparticle systems [7-9].

Thus, our contribution aims to comprehensively explore the impact of the Atomic Layer Deposition (ALD) process of metal oxides on the magnetic signal, structure, and composition of iron oxide supraparticles. Through detailed Mössbauer analysis, we will demonstrate the oxidation-shielding properties afforded by specific metal oxides. Finally, using the Small-Angle Neutron Scattering with incident beam Polarization (SANSPOL) we will reveal the absence of intra-supraparticle structural displacement during the ALD process, along with increased internal ordering and a significant reduction in the magnetic "dead layer" size.

1. J. E. Lee et al. Accounts Chem. Res. 44 893–902 (2011).
2. N. C. Bigall et al. Nano Today 7 282–296 (2012).
3. A. G. Dong et al. Nature 466 474–477 (2010).
4. T. Wang et al. Science 338 358–363 (2012).
5. J. Guo et al. Advanced Materials 25 5196-5214 (2013).
6. Z. D. Lu et al. Chem. Soc. Rev. 41 6874–6887 (2012).
7. S. Müssig, V. B. Koch et al. Small Methods 6, 2101296, (2022).
8. P. Groppe, et. al. Chemistry of Materials 2025 37 (8), 2815-2826 (2025).
9. S. Mussig et al. doi:10.5291/ILL-DATA.5-61-48.

L42

MAGNETIC MORPHOLOGY OF MULTISHELL NANOPARTICLES

Š. Hricov[1], O. Kaman[2], I. Dirba[3], N. J. Steinke[4], D. Zákutná[4,5]

[1]Department of Condensed Matter Physics, Faculty of Mathematics and Physics, Charles University, Ke Karlovu 5, 121 16 Prague 2, Czechia

[2]Institute of Physics of the Czech Academy of Sciences, Cukrovarnická 10, 162 00 Prague 6, Czechia

[3]Technical University of Darmstadt, Karolinenplatz 5, 64289 Darmstadt, Germany

[4]Institut Laue-Langevin, 71 Avenue des Martyrs CS 20156, 38042 Grenoble, France

[5]Department of Inorganic Chemistry, Faculty of Science, Charles University, Hlavova 8, 128 00 Prague 2, Czechia

Magnetic nanoparticles (MNPs) are of high research interest due to their unique physical properties, which lay the foundation for various applications, ranging from biomedical diagnostics and therapeutic interventions to high-density data storage systems and environmental remediation processes. Broadly known and well-studied materials of this class are iron oxides MNPs. Among other research interests, they have been heavily exploited for their heating abilities via magnetic fluid hyperthermia. This process is a cornerstone for innovative cancer treatment therapies, which aim to localise tumour elimination. However, we propose a novel candidate material, the ε-Fe_3N. It possesses unprecedented magnetic properties, essentially surpassing the well-established iron oxide MNPs [1], having larger saturation magnetization, leading to better heating performance in hyperthermia. As a result, the required therapeutic temperatures for tumour ablation can be achieved with a less concentrated MNP dispersion, thereby reducing the dose needed. Nevertheless, due to the

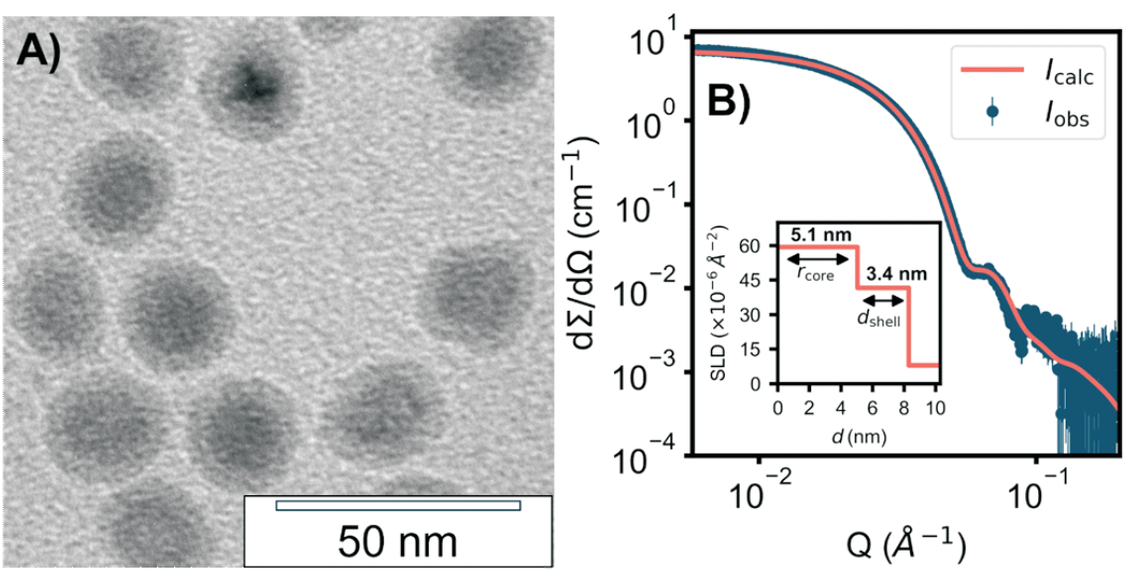

Figure 1. A TEM micrograph of passivated ε-Fe_3N MNP, **B** SAXS curve recorded on dispersion of passivated ε-Fe_3N MNP.

sults in massive oxidation. Thus, a robust surface protection must be realised. While considering the potential biomedical applications, we propose a silica encapsulation procedure to hinder ε-Fe_3N oxidation and to establish biocompatibility, together with possibility to form aqueous dispersions. To successfully grow a silica layer, we have chosen a route of ε-Fe_3N surface passivation, which we present in this contribution, together with insight into magnetic behaviour of complex core@shell MNPs. The bright-field transmission electron microscope micrographs (**Figure 1: A**) and small-angle X-ray scattering (**Figure 1: B**) show well-defined core@shell MNP morphology of the passivated nanoparticles with a mean particle diameter of 17.2(2) nm. Nevertheless, the macroscopic magnetization measurements revealed unexpected behaviour leading to a decrease in saturation magnetization and the presence of exchange bias at 5 K. To further explore, the complex magnetic nature of this material was disentangled by probing magnetic scattering fluctuations using the magnetic small-angle neutron scattering with incident beam polarization at the D33 instrument at ILL [2]. Finally, we will disentangle the magnetic morphology contributions from the magnetic core and shell part of passivated ε-Fe_3N MNPs and discuss the resulting magnetic response of the presented MNPs in detail.

1. I. Dirba et al., J. Phys. D: Appl. Phys, 56, 025001 (2023). doi: 10.1088/1361-6463/aca0a9.
2. Š. Hricov et al., Unmasking the Complex Core-Multishell Morphology of Magnetic Nanoparticles. Institut Laue-Langevin, proposal No. DIR-297 (2023). doi: 10.5291/ILL-DATA.DIR-297

This work was supported by the Czech Science Foundation (22-10035K) and the AMULET project, co-funded by MŠMT and the EU (CZ. 02.01.01/00/22_008/0004558). We also acknowledge the Institut Laue-Langevin for beamtime and financial support.

Session XII - September 11, Thursday

L43

LAUEDB: A DATASET FOR LAUE PATTERNS

Štěpán Venclík, Tomáš Červeň, Jan Kříž, David Sviták, Petr Čermák

Charles University, Prague, Czech Republic

Laue diffraction is a widely used technique for orienting single crystals and a routine procedure during sample preparation for many scientists. Over the years, a variety ofsoftware tools have been developed to assist in interpreting Laue patterns [1, 2]. Despite significant progress in image processing and pattern recognition, a robust and fully automated solution for indexing Laue patterns has yet to be achieved.

In recent years, **machine learning** has emerged as a promising approach to tackle this challenge [3]. However, the development and validation of more advanced algorithms are currently hindered by the lack of annotated experimental datasets. As a result, all training and testing are still conducted exclusively on synthetic data.

LaueDB aims to bridge this gap by creating a **dataset of oriented X-ray and neutron Laue patterns** that could serve as a training and evaluation dataset for both classical and machine learning approaches.

We plan to utilise the Automatic Laue Sample Aligner (ALSA) [4] to create the initial dataset, capturing a large number of patterns for each sample crystal, as well as collaborate with research infrastructures to develop a submission pipeline for patterns created during routine sample orientation. In addition, existing tools and algorithms for peak finding and Laue indexing will be compared.

1. Esmeralda Laue Suite (https://code.ill.fr/scientific-software/esmeralda).
2. Clip4 (https://clip4.sourceforge.net/)
3. Purushottam Raj Purohit, R. R. P., Tardif, S., Castelnau, O., Eymery, J., Guinebretiere, R., Robach, O., Ors, T. & Micha, J.-S. (2022). J. Appl. Cryst. 55, 737-750.
4. ALSA (https://charlesautomata.cz/alsa).

L44

PSB_GUI – MATLAB ROUTINE FOR THE REFINEMENT OF RESIDUAL STRESSES, MICROSTRAIN AND CRYSTALLITE SHAPE IN CUBIC MATERIALS

Petr Cejpek[1,2], David Rafaja[2]

[1]*Institute of Physics, Czech Academy of Sciences, Na Slovance 1999/2, 182 00 Praha 8, Czech Republic*
[2]*Institute of Materials Science, TU Bergakademie Freiberg, Gustav-Zeuner-Str. 5, 09599 Freiberg, Germany*

Residual stress is commonly determined from the shift of X-ray diffraction (XRD) lines using the of $\sin^2\psi$ method. Microstrain and grain sizes are typically evaluated from the line broadening and Williamson-Hall plot. This standard procedure is mainly applied to polycrystalline materials or thin films. Regarding grain or crystallite shapes, the spherical shape is usually sufficient enough.

However, in many cases, more complex theoretical models are required to achieve a reasonable fit of the experimental data. Moreover, such situations can occur even in relatively simple systems like thin Mo film deposited on single-crystalline MgO(100) substrate [1]. As the result of the minimisation of deformation energy, Mo forms a hetero-epitaxially grown matrix along with the twins that are specifically oriented with respect the Mo matrix. Therefore, the approach related to the family of crystallites method [2] needs to be applied during the refinement. This requires the experimental data correctly separated into groups and the diffraction peaks need to be precisely indexed. Each group is then assigned to different theoretical models for XRD line shift and broadening refinement, since the different families of crystallites can exhibit different properties. For example, different components of the residual stress or asymmetric shapes of crystallites grown in the specific crystallographic directions.

For this purpose, the Matlab routine *PSB_GUI* (with a graphical user interface) has been developed. It enables a complex refinement of XRD line shift and broadening for cubic materials. The routine allows the separation of the datapoints into groups and each of these groups can be associated with its own unique combination of theoretical models for residual stress, microstrain and grain sizes. For XRD line shift refinement, the following models are supported: Voigt, Reuss, Vook-Witt, stress factors for textured polycrystals or the possibility to refine individual stress components. [3] For the line broadening, models include spherical crystallites, cylindrical and ellipsoidal crystallites grown in specific crystallographic directions, stacking faults, isotropic microstrain, and anisotropic microstrain connected to dislocations [4] or specific directions of Burgers vectors.

To run *PSB_GUI* properly, Matlab along with the Optimalisation toolbox is required. The entire routine is currently available on GitHub at the following link: *https://github.com/PetrCejpek/PSB_GUI*.

1. Cejpek, P., et al. Lattice strain relaxation in thin Mo films grown heteroepitaxially on MgO single crystals, Journal of Applied Crystallography, under review.
2. Kužel, R., et al. Complex XRD microstructural studies of hard coatings applied to PVD-deposited TiN films. Part I: Problems and methods, Thin Solid Films **247** (1994), 64–78, https://doi.org/10.1016/0040-6090(94)90477-4.
3. Welzel, U., et al. Stress analysis of polycrystalline thin films and surface regions by X-ray diffraction, Journal of Applied Crystallography **38** (2005), 1–29, https://doi.org/10.1107/S0021889804029516.
4. Ungár, T., et al. The contrast factors of dislocations in cubic crystals: the dislocation model of strain anisotropy in practice, Journal of Applied Crystallography **32(5)** (1999), 992–1002, https://doi.org/10.1107/S0021889899009334.

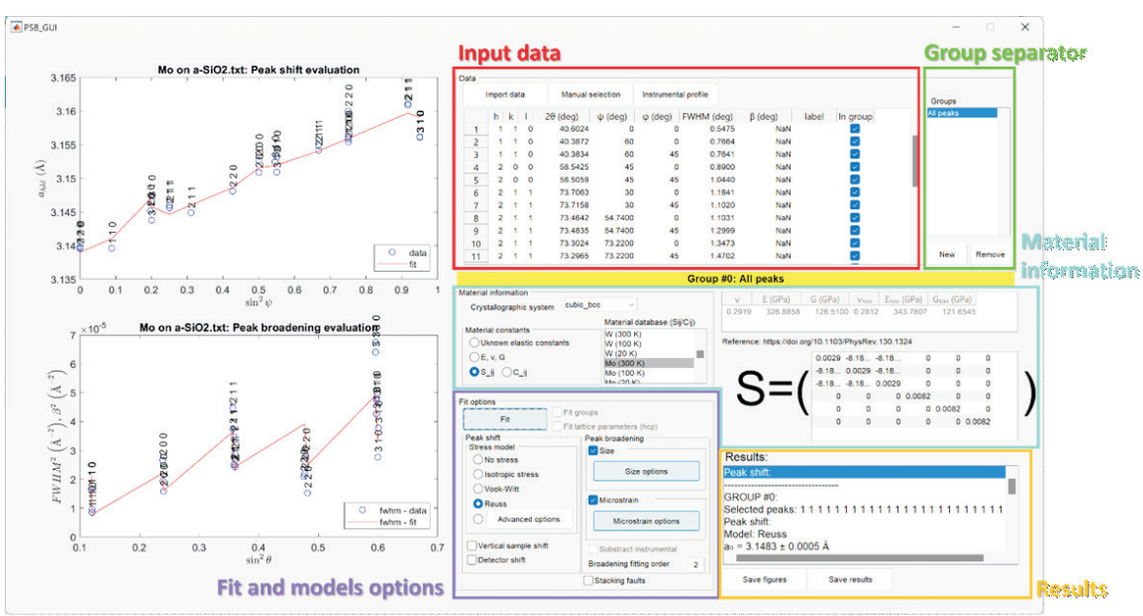

Figure 1. Overview of the PSB_GUI main window.

L45

EFFECTS OF HEAT TREATMENT ON MICROSTRUCTURE, PORE MORPHOLOGY, AND MICROMECHANICAL PROPERTIES OF AM-PRODUCED TI6AL4V ALLOY

Ubaid Ahmed[1,2] A. Bhardwaj[1], Miroslav Lebeda[1], J. Kopeček[1], Daniel Šimek[1]

[1]FZU, Institute of Physics of the Czech Academy of Sciences, Na Slovance 2, Prague 8, 182 21, Czech Republic

[2]Department of Condensed Matter Physics, Charles University, Prague, Czech Republic

Ti6Al4V, a grade 5 titanium alloy, is widely utilized in aerospace, biomedical, marine, and energy sectors due to its high strength-to-weight ratio, superior corrosion resistance, and excellent biocompatibility. With the advent of advanced manufacturing techniques such as Additive Manufacturing (AM), the production of intricate geometries has become more efficient compared to traditional methods. However, the localized thermal gradients generated during AM processes significantly influence the microstructure, pore morphology, and mechanical properties of the material. This study investigates the effects of heat treatment on the microstructure, pore morphology, and micromechanical properties of AM-produced Ti6Al4V specimens.

Using Micro-Computed Tomography (Micro CT) and X-ray Diffraction (XRD), pore defect volumes, distributions, equivalent spherical diameters, and sphericity coefficients were analysed under three heat treatment conditions (550 °C, 750 °C, and 1150 °C). The average pore volumes were found to be 1.975×10^{-4} mm^3, 1.2838×10^{-4} mm^3, and 4.347×10^{-5} mm^3 for the as-cast and heat-treated samples at 550 °C, 750 °C, respectively. The mean sphericity values were 0.747, 0.749, and 0.921, indicating improved pore uniformity and shape at 750°C.

Hardness measurements revealed values up to 7.17 GPa, while the reduced modulus values up to 139.57 GPa. The results demonstrate that annealing at 750 °C achieved the most favourable balance between reduced pore volume and uniformity, attributed to stabilization of the alpha phase and atomic diffusion minimizing surface energy. Additionally, at this temperature, the mechanical properties were improved, providing a balance between strength and elasticity. These findings highlight the potential of heat treatment optimization to enhance the performance of AM-produced Ti6Al4V for demanding applications.

L46

Microstructure of rotary swaged copper bars with carbon admission

MIKROSTRUKTURA MĚDĚNÝCH, ROTAČNĚ KOVANÝCH TYČÍ S PŘÍMĚSÍ UHLÍKATÉ FRAKCE

J. Kopeček[1*], L. Kunčická[2], T. Kmječ[1], J. Walek[2], D. Šimek[1], U. Ahmed[1], J. Duchoň[1], A. Bhardwaj[1] and R. Kocich[2]

[1]FZU – Institute of Physics of the Czech Academy of Sciences, Praha, Czech Republic,

[2]Faculty of Materials Science and Technology, VŠB–Technical University of Ostrava, Ostrava-Poruba, Czech Republic

Jednou z hlavních aplikačních oblastí mědi jsou elektrické vodiče, což je odrazem jejích výborných vodivostních vlastností [1]. Náležitě čistá a vyžíhaná měď má excelentní vodivost, která však klesá vlivem příměsových atomů, stejně jako vlivem plastické deformace. Přesto byla pozorována výborná vodivost materiálů připravených některými metodami značné plastické deformace, které vedou k tvorbě nanodvojčat [2]. Jednou z metod, kterou je možné připravit takovou mikrostrukturu je rotační kování [3].

V prezentované práci se věnujeme materiálům připraveným kompaktizací prášku se sférickými zrníčky a příměsí uhlíkaté fáze deponované na povrch prášků. Koncept vychází z předchozích experimentů s kováním kompaktní čisté mědi [4,5] a materiálů připravených kompaktizací prášků s příměsí oxidů [6]. Elektrické vodivost takto připravených materiálů v ose kování přesahuje vodivost konvenčně žíhané mědi IACS (International Annealed Copper Standard).

Vykované tyče připravené na VŠB – TU Ostrava byly použity pro přípravu metalografických vzorků, případně dále žíhány a všechny stavy byly standardně zkoumány pomocí SEM (Tescan FERA 3), EDS a EBSD (EDAX Octane super 60 mm^2 a Digiview IV), TEM (Jeol JEOL 2000 FX) a XRD (Panalytical X´Pert). Pro vyhodnocení mikrostruktury pomocí EBSD byl použit software OIM 9 využívající sférických harmonických funkcí pro určení orientace krystalové mříže.

Potvrdili jsme, že rotační kování prášků s obsahem uhlíkaté fáze vede ke vzniku textury s komponentami ⟨100⟩ a ⟨111⟩ v ose kování, což je podobné chování jaké bylo pozorováno u kování při teplotě kapalného dusíku, které vytváří silnou texturu ve směru ⟨111⟩ v ose kování, složka

ve směru ⟨100⟩ je oproti čistému materiálu výrazně slabší. Zrna jsou ve směru osy tyče protažena, ale jsou významně kratší než v kovaném materiálu. Pomocí TEM byly pozorovány dislokace v kovaném materiálu, avšak nikoli precipitáty. Zaměřili jsme se také na směrovou závislost elektrické vodivosti vzhledem k osám kování.

1. J. R. Davies (Ed), ASM Specialty Handbook, Copper and Copper Alloys, Materials Park, ASM International, 2001.
2. L. Lu, Y.F. Shen, X.H. Chen, L.H. Qian, K. Lu, Ultrahigh strength and high electrical conductivity in copper, Science, 304 (2004), 422-426.
3. X. Ke, J. Ye, Z. Pan, J. Geng, M.F. Besser, D. Qu, A. Caro, J. Marian, R.T. Ott, Y.M. Wang, F. Sansoz, Ideal maximum strengths and defect-induced softening in nanocrystalline-nanotwinned metals, Nature Materials, 18 (2019), 1207-1214.
4. J. Kopeček, L. Bajtošová, P. Veřtát, D. Šimek, *(Sub)structure Development in Gradually Swaged Electroconductive Bars*, Materials, 16 (2023) 5324-1 – 5324-12.
5. R. Kocich, L. Kunčická, Crossing the limits of electric conductivity of copper by inducing nanotwinning via extreme plastic deformation at cryogenic conditions, Mat. Char. 207 (2024) 113513.
6. L. Kunčická, J. Walek, R. Kocich, Deformation Behavior of La_2O_3-Doped Copper during Equal Channel Angular Pressing, Adv. Eng. Mater. (2024) 2402412.

We acknowledge Czech Science Foundation project 25-16860S and CzechNanoLab Research Infrastructure (LM2023051) by MEYS CR support.

Session XIII - September 12, Friday

L47

Y-HEXAFERRITE THIN FILMS DEPOSITED BY CHEMICAL SOLUTION DEPOSITION ON DIFFERENT SUBSTRATES STUDIED BY XRD

Radomír Kužel[1], Milan Dopita[1], Lukáš Horák[1], Josef Buršík[2]

[1]Charles University, Faculty of Mathematics and Physics, Ke Karlovu 5, Praha 2 121 16, Czech Republic,
[2]Institute of Inorganic Chemistry of the Czech Academy of Sciences, v.v.i., Husinec-Řež 1001, 250 68, Czech Republic
radomir.kuzel@matfyz.cuni.cz

Thin films of several phases of hexagonal ferrites with a potential of magnetoelectric effect (ME) were prepared by a chemical solution deposition method, and the number of processing parameters was tested and optimized with the of minimizing the amount of impurities that could spoil the magnetic properties of the final material. With the aim of preparation of highly oriented ferrite films, several substrates were used, and different substrate/seeding layer/ferrite layer architectures were proposed. [1-5].

The mechanism of ME in Y-type hexaferrite films appears to be significantly influenced by lattice parameters. New Y-ferrite phases were prepared with the composition $Ba_xSr_{2-x}Co_2Fe_{11.1}Al_{0.9}O22$, and it was found that the magnetic structure is non-colinear ferrimagnetic type. These films could be prepared with good out-of-plane and in-plane orientation directly on STO - SrTiO (111) substrate, but the M-phase seeding layer usually leads to better results. The ME effect was identified to be maximum for equal content of barium and strontium but the dependence on *x* is now studied in more detail. In the project, we investigate the influence of the degree and type of preferred orientation of the films as well as their real structure on the

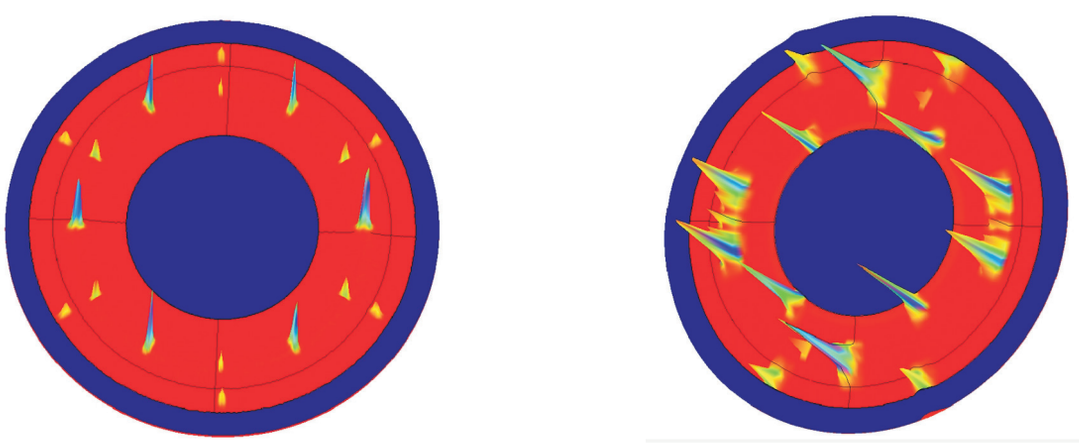

Figure 1. Illustrations of preferred orientation of Y-films. Partial pole figures (119) for the film grown on $MgAl_2O_4$ (111) substrate (left), and (024) for the film grown on Al_2O_3 *a*-cut.

ME effect. By using different substrates, different preferred orientations and strains can be obtained.

Symmetrical θ–θ scans often indicated a strong preferred orientation (000*l*) on STO (111). This is the so-called out-of-plane orientation. In case of fiber texture, its degree can be well characterized by the ω scans (rocking curves). For the estimation of the alignment of planes perpendicular to the substrate, measurement of additional asymmetric Bragg reflections is necessary, simply by the φ scans (rotation on the axis perpendicular to the film plane). The lattice parameters of the films were obtained by evaluating the maxima positions of about 30 diffraction profiles measured at different sample inclinations and Ö angles corresponding to the maxima, i.e., by creating a powder-like pattern [6].

Several sets of Y-films were investigated. Films with different thicknesses were deposited on the STO substrate with orientations (111), (110), (100), and ceramics. In all cases, (00*l*) textures of Y-phases of different degrees were observed but only for (111) also a strong (111) texture was detected, as it can be expected. Then other substrates were used - MgO (111), $LaAlO_3$ (111) - LAO, stabilized cubic zirconia (ZrO_2) and $MgAl_2O_4$ (111). In this case, significant out-of-plane and in-plane orientations of Y-films were observed for LAO substrates with FWHMs of both ω and Ö scans of approximately 0.4°. For MgO substrates both orientations were also indicated with a slightly wider FWHMs (over 1°). On zirconia, the preferred orientations are relatively poor with clear domains in in-plane orientations. Another set of substrates used were differently oriented sapphire substrates (rhombohedral Al_2O_3) – *c*-cut (000*l*), *a*-cut (11-20), *m*-cut(10-10), *r*-cut (1-120). It seems that different pronounced textures of Y-hexaferrites can grow there including the (*h*00) orientation on *a*-cut of substrate, or (*hh*0) on *m*-cut of substrate. Some illustrations of preferred orientation with a few domains are shown in Fig. 1.

1. Shin, KW; Soroka, M.; Shahee, A; Kim, KH; Buršík, J.; Kužel, R; Vronka, M; Aguirre, MH: *Advanced Electronic Materials.* v. **8** (2022). 2101294.
2. J. Buršík, R. Uhrecký, D. Kaščáková, M. Slušná, M. Dopita, R. Kužel, *Journal of the European Ceramic Society* **36** (2016) 3173–3183.
3. R. Uhrecký, J. Buršík, M. Soroka, R. Kužel, J. Prokleška , *Thin Solid Films*. **622** (2017) 104–110.
4. M. Soroka, J. Buršík, R. Kužel, J. Prokleška, M.H. Aquirre, *Thin Solid Films,* **726** (2021) 138670.
5. M. Soroka, J. Buršík, R. Kužel, L. Horák, J. Prokleška, M. Vronka & V. Laguta. *Journal of European Ceramic Society.* **43**, (2023) 6916-6924.
6. R. Kužel, J. Buršík, M. Dopita, L. Horák, M. Soroka, *Materials Structure* **30** (2024) 328-331.

The authors appreciate the support by the grant of the Czech Grant Agency, no. 24-12710S.

Monday, September 8

13:00 Opening

13:15-15:25 Session I

Chairs: Milan Dopita, Jaromír Kopeček

13:15
František Laufek *(Czech Geological Survey, Praha)*
Minerals within the Pd-Ni-As system: Crystal structures

13:45
Zdeněk Jansa *(New Technologies-Research Centre, Plzeň)*
Phase analysis of soil sediments with respect to presence asbestos minerals

14:10
Cristian Pilloni *(Faculty of Science, Charles University - CU, Praha)*
Properties of schwertmannite: The critical role of phase purity

14:35
Esther de Prado *(Institute of Physics, Czech Academy of Sciences - CAS, Praha)*
Improving thermoelectric efficiency of multilayer ScN/$Sc_{1-x}Nb_xN$ heterostructures by Nb doping

15:00
Jan Drahokoupil *(Institute of Physics, CAS, Praha)*
$BaTiO_3$/$LaNiO_3$ thin films: From diffraction to computer simulations

15:25 Break, refreshment

15:50-17:30 Session II

Chairs: Stanislav Daniš, Nikolaj Ganev

15:50
Petr Machovec *(Faculty of Mathematics and Physics, CU, Praha)*
Halide segregation in mixed-halide perovskites studied by XRD

16:15
Dominik Farka *(Faculty of Science, University of South Bohemia in České Budějovice)*
Thiophene-based conductive polymers: Structural order vs. charge-Transport

16:40
Petr Doležal *(Faculty of Mathematics and Physics, CU, Praha)*
Polymorphs of $Zn_xCu_{4-x}(OH)_6Cl_2$ and their physical properties

17:05
Jamil Eduardo Flores Gonzales *(Institute of Physics, CAS, Praha)*
Diffuse scattering in $(K,Na)NbO_3$ solid solutions

17:30-19:30 Short courses

Real structure and total powder pattern fitting – Introduction (R. Kužel, Z. Matěj)

MSTRUCT course (M. Dopita, L. Horák, Z. Matěj)

Moorhen course (Lucrezia Catapano, Petr Kolenko)

19:30 Dinner

20:30 Courses

Tuesday, September 9

7:00-8:30 Breakfast

8:30-10:30 Session III

Chair: Václav Holý

8:30
Stanislav Daniš *(Faculty of Mathematics and Physics, CU, Praha)*
Data and what to do with it

9:15
Vojtěch Chlan *(Faculty of Mathematics and Physics, CU, Praha)*
Nuclear magnetic resonance in solids

10:00
Lukáš Horák *(Faculty of Mathematics and Physics, CU, Praha)*
Selected examples in X-ray reflektometry

10:30 Break, refreshment

11:00-12:30 Session IV

Chair: Jaroslav Maixner

11:00
Michal Dušek *(Institute of Physics, CAS, Praha)*
First experience with single crystal diffractometer Synergy R

11:25
Jiří Zelenka *(Institute of Physics, CAS, Praha)*
Interpretation of electron density maps using neural networks

11:50
Jan Rohlíček *(Institute of Physics, CAS, Praha)*
Use of intermolecular distances in solving structures from powders

12:30 Lunch

14:00-15:45 Session V

Chair: Petr Pachl, Petr Kolenko

14:00
Jindřich Hašek *(Institute of Biotechnology, CAS, Vestec)*
Protein Crystallization

14:30
Jan Dohnálek *(Institute of Biotechnology, CAS, Vestec)*
Information on protonation in biomolecular structures

14:55
Bohdan Schneider *(Institute of Biotechnology, CAS, Vestec)*
Advances in annotation and validation of nucleic acids

15:20
Jiří Brynda *(Institute of Organic Chemistry and Biochemistry, CAS, Praha)*
Advances in annotation and validation of nucleic acids

15:45 Break, refreshment

Tuesday, September 9	Wednesday, September 10
15:45 Break, refreshment	**7:00-8:30** Breakfast
16:15-17:20 Session VI *Chairs: Jan Dohnálek, Bohdan Schneider*	**8:30-10:00 Session VII** *Chair: Daniel Šimek*
16:15 **Petr Kolenko** *(Faculty of Nuclear Sciences and Physical Engineering, Czech Technical University, Praha)* Crystal structure of PROSS-edited human interleukin 24 **16:40** **Barbora Kaščáková** *(Faculty of Science, University of South Bohemia in České Budějovice)* Characterization of PROTAC-508: A cereblon-recruiting degrader of enteroviral 2A protease **16:55** **Petra Havlíčková** *(Faculty of Science, University of South Bohemia in České Budějovice)* Beyond oncogenes: How ras–MAPK variants Influence neurodevelopment	**8:30** **Václav Holý** *(Faculty of Mathematics and Physics, CU, Praha)* Hard x-rays with orbital momentum, properties and dynamical diffraction **9:10** **Jozef Bednarčík** *(University of P.J. Šafárik, Košice)* Study of local atomic structure of disordered materials by in-situ synchrotron experiments **9:35** **Milan Dopita** *(Faculty of Mathematics and Physics, CU, Praha)* Light-induced phase segregation and structural relaxation in mixed-halide perovskites. FeOH nanoparticles
17:30 **Radomír Kužel** Information on preparation of ECM-36	**10:00** **Jiří Špringer** *(Anton Paar)* Anton Paar, SAXSpoint 500/700 – new equipment for small-angle scattering **10:20** **Szymon Stolarek** *(Xenocs, SAS)* Enabling nanoscale insight: Advanced X-ray scattering solutions from Xenocs
17:40-19:20 **Jan Walla, Boris Míč** *(Měřící technika Morava)* Practical demonstration of table-top diffractometer D6 Phaser	
19:30 Dinner	**10:40** Break, refreshment
20:30 Meeting of CSCA board	**11:10-13:15 Session VIII** *Chairs: Jan Rohlíček, Michal Dušek*
	11:10 **Pawel Olowek** *(Rigaku)* XSPA: the future of XRD **11:30** **Stjepan Prugovečki** *(Malvern Panalytical)* New functions of XRD Empyrean
	11:50 **Miroslav Lebeda** *(Institute of Physics, CAS, Praha)* XRDlicious: An online tool for powder diffraction pattern and RDF simulation from crystal structures **12:15** **Zdeněk Matěj** *(Max IV Laboratory, Lund, Sweden)* Basic crystallographic algorithms in the ML language **12:45** **Jan Drahokoupil, Miroslav Lebeda** *(Institute of Physics, CAS, Praha)* Introduction to Mace course
	13:15 Lunch
	14:30 CSCA assembly
	15:30 Departure to Nová Bystřice **16:00** Excursion in museum of old American cars and brewery
	18:30 Raut in Číměř, guesthouse Life

Thursday, September 11

7:00-8:30 Breakfast

8:30-10:30 Session IX - Large European Neutron Facilities

Chair: Milan Klicpera

8:30
Mark Johnson *(ILL Grenoble, France)*
Institute Laue-Langevin - instrument and infrastructure upgrades, the science strategy and new research opportunities

9:10
Michael Hofmann *(MLZ Munich, Germany)*
Diffraction at MLZ

9:50
Přemysl Beran *(ESS), Lund, Sweden*
ESS News and first science oportunities

10:30 Break, refreshment

11:00-12:30 Session X - Neutron Science in Czech Republic 1

Chair: Přemysl Beran

11:00
Jan Šaroun *(Institute of Nuclear Physics, CAS, Řež)*
Neutron diffraction laboratory in Řež and its user program

11:20
Milan Klicpera *(Faculty of Mathematics and Physics, CU, Praha)*
Czech neutron association - establishment, mission, and objectives

11:30
Pavel Strunz *(Institute of Nuclear Physics, CAS, Řež)*
Residual-stress distribution in components fabricated with involvement of additive manufacturing

Olena Levytska, Pavel Strunz *(Institute of Nuclear Physics, CAS, Řež)*
Validation of contour cut model for residual stresses in AM-repaired simulated defect by neutron diffraction

12:00
Jiří Kulda *(ILL Grenoble, France)*
Pump-probe inelastic neutron scattering experiments

12:30 Lunch

14:00-16:00 Session XI - Neutron Science in Czech Republic 2

Chairs: Pavel Strunz, Jan Šaroun

14:00
Gergely Farkas *(Institute of Nuclear Physics, CAS, Řež)*
Experimental determination of critical resolved shear stresses by neutron diffraction

14:20
Vasyl Ryukhtin *(Institute of Nuclear Physics, CAS, Řež)*
Investigations of vortex lattices and skyrmions using neutron scattering

14:40
Filip Hájek *(Faculty of Mathematics and Physics, CU, Praha)*
Novel pyrochlore-derived structure in rare-earth iridate single crystals

Thursday, September 11

15:00
David Sviták *(Faculty of Mathematics and Physics, CU, Praha)*
Magnetic structure and excitations in the antiferromagnet $Na_2BaMn(PO_4)_2$

15:20
Romain Conan *(Faculty of Science, CU, Praha)*
Magnetic correlation in functionalized supraparticles

15:40
Štefan Hricov *(Faculty of Mathematics and Physics, CU, Praha)*
Magnetic morphology of multishell nanoparticles

16:00 Break, refreshment

16:20-17:40 Session XII

Chairs: Pavla Roupcová, Zdeněk Matěj

16:20
Štěpán Venclík *(Faculty of Mathematics and Physics, CU, Praha)*
LaueDB: A dataset for Laue patterns

16:40
Petr Cejpek *(Institute of Physics, CAS, Praha)*
PSB_GUI – Matlab routine for the refinement of residual stresses, microstrain and crystallite shape in cubic materials

17:00
Ubaid Ahmed *(Institute of Physics, CAS, Praha)*
Effect of Heat Treatment on Ti6Al4V porosity and micromechanical behavior

17:20
Jaromír Kopeček *(Institute of Physics, CAS, Praha)*
Microstructure of rotary swaged copper bars with carbon admission

17:40-19:30 Course Mace (Miroslav Lebeda, Jan Drahokoupil)

19:30 Dinner

Friday, September 12

7:00-8:30 Breakfast

9:00-9:30 Session XIII

Chair: Milan Dopita

9:00
Radomír Kužel *(Faculty of Mathematics and Physics, CU, Praha)*
Hexaferrite thin films prepared on different and differently oriented substrates studied by XRD

9:30 Closing

9:40 Possible continuation of courses

Contents

Abstracts from Struktura 2025

Author Index

Materials Structure **Bulletin Krystalografické společnosti**
Vydává a rozšiřuje Krystalografická společnost. Tiskne Karel Hájek designhhstudio.
S podporou Akademie věd ČR.
Adresa sekretariátu redakce: R. Kužel, MFF UK, Ke Karlovu 5, 121 16 Praha 2
Technická redakce: I. Kutá Smatanová, R. Kužel
ISSN 1211 – 5894 díl **31** (2025), číslo 2 CSCA

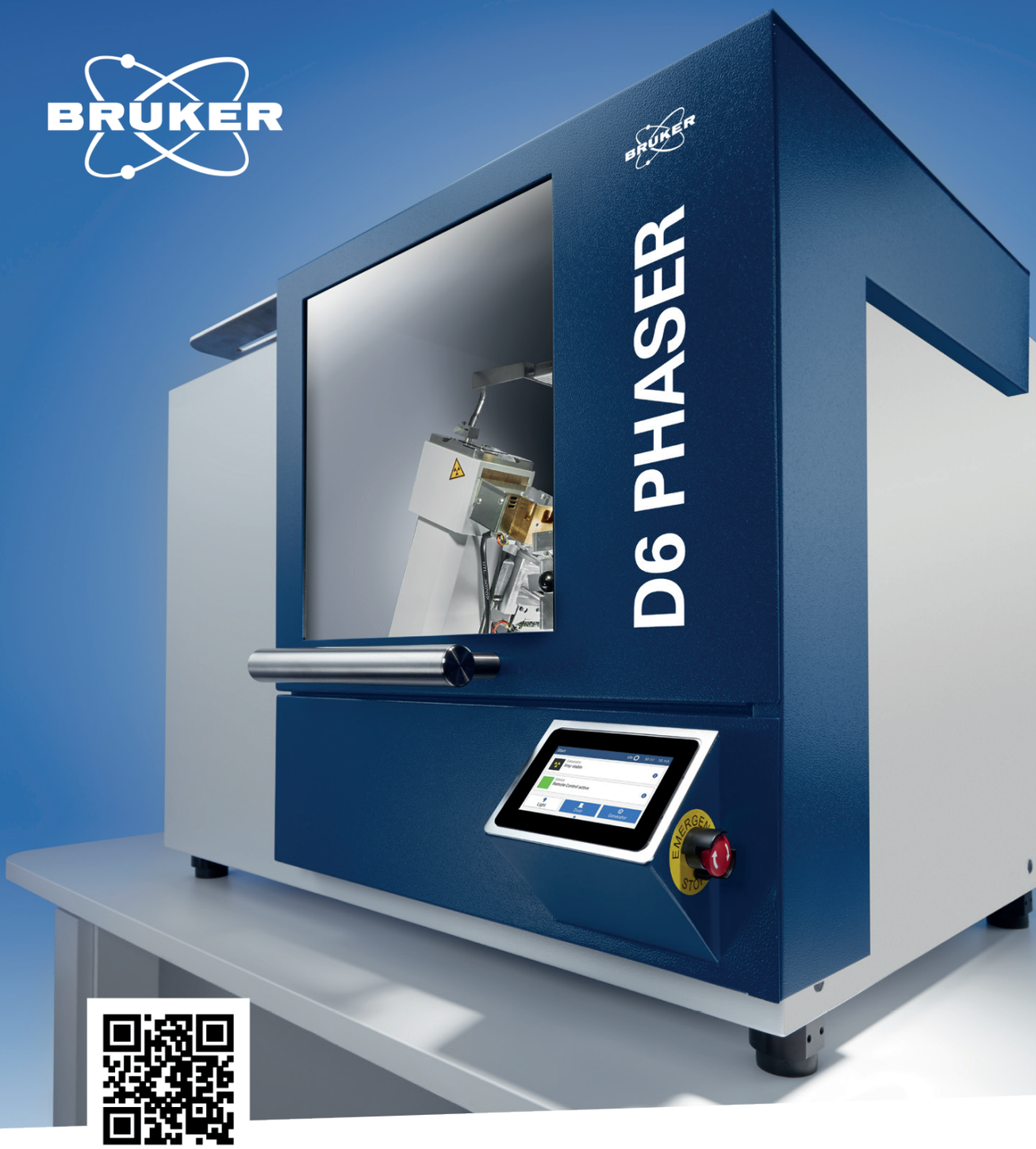

X-RAY DIFFRACTION

D6 PHASER - The Benchtop Platform

Powerful. Versatile. Accessible.

- Up to 1.2 kW with internal cooling + LYNXEYE XE-T detector + Motorized beam optics
- Reflection and transmission powder XRD + Non-ambient powder diffraction + GID, XRR, Stress, Texture
- Dynamic Beam Optimization + Touch panel operation + Stage and optics exchange

Discover more at **bruker.com/d6phaser**

Anton Paar

Next-Level Sample Handling
for Every XRD Challenge

XRDynamic Autosampler

The XRDynamic Autosampler enhances Anton Paar's XRD solutions with high sample capacity, seamless integration, and flexible performance. Combined with XRDynamic 500, it enables efficient, automated measurements for all sample types with consistently reliable results.

FIND OUT MORE

www.anton-paar.com/apb-xrd-autosampler

Discover Xenocs SAXS/WAXS solutions.

Our mission : to provide solutions for nanoscale characterization of materials

Xeuss Pro

Nano-inXider

Xenocs provides advanced X-ray solutions (SAXS/WAXS, Imaging) for nanoscale characterization of materials. With 25 years of innovation, we support academic and industrial R&D labs worldwide with high-performance instruments, powerful software, and dedicated customer service. Headquartered in France, Xenocs operates globally through subsidiaries and local partners.

www.xenocs.com

xenocs
Exploring the very small

11th European Conference on Residual Stresses

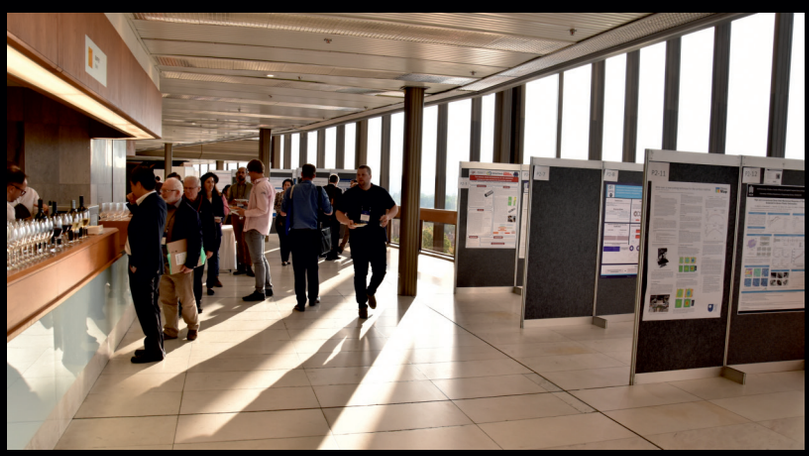

Praha, KCP
3.6.-7.6. 2024

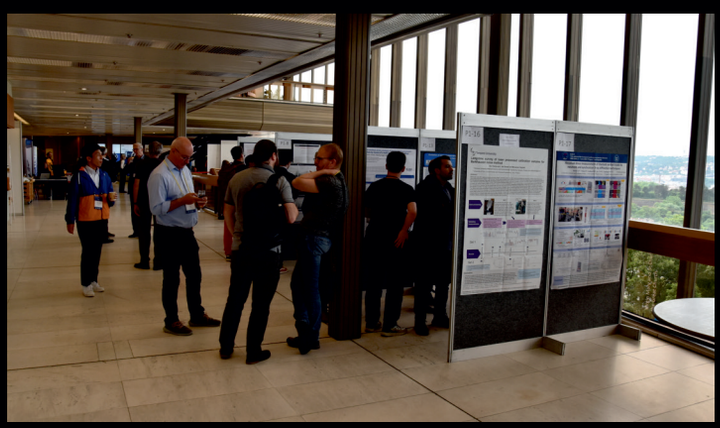

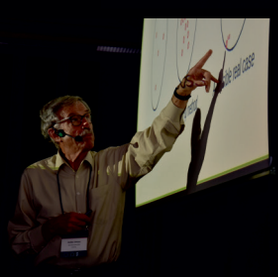

learn more

EMPYREAN

THE INTELLIGENT DIFFRACTOMETER

Learn More

With the 3rd generation Empyrean, we have now redefined the concept of a multipurpose diffractometer: our newly designed MultiCore Optics enable the largest variety of measurements without any manual intervention.

Empyrean has the unique ability to measure all sample types - from powders to thin films, from nanomaterials to solid objects - on a single instrument.

The world of materials science is constantly changing and the life of a high performance diffractometer is much longer than the typical horizon of any research project.

With Empyrean, you are ready for anything the future holds.

www.malvernpanalytical.com/empyrean

Malvern Panalytical
a spectris company

www.malvernpanalytical.com

www.rigaku.com

www.anton-paar.com

www.xenocs.com

www.dectris.com